Author/s:
Guo, Y;Hu, G;Chen, K;Guo, J;Webley, PA;Li, GK

Title:
Capture of dilute methane with a novel dynamic-feed dual-reflux pressure swing adsorption process

Date:
2022-01-01

Citation:
Guo, Y., Hu, G., Chen, K., Guo, J., Webley, P. A. & Li, G. K. (2022). Capture of dilute methane with a novel dynamic-feed dual-reflux pressure swing adsorption process. Aiche Journal, 68 (1), https://doi.org/10.1002/aic.17390.

Persistent Link:
https://hdl.handle.net/11343/298845

Guo Yalou (Orcid ID: 0000-0003-3551-7782)

Hu Guoping (Orcid ID: 0000-0002-7480-8411)

Capture of Dilute Methane with a Novel Dynamic-Feed Dual-Reflux Pressure Swing Adsorption Process

Yalou Guo, Guoping Hu, Kaifei Chen, Jining Guo, Paul A. Webley, Gang (Kevin) Li

Department of Chemical Engineering, The University of Melbourne, Parkville, VIC 3010, Australia

Corresponding authors: li.g@unimelb.edu.au

Abstract

Dual-reflux pressure swing adsorption (DR-PSA) is a state-of-art adsorption technology claiming to achieve both high product purity and recovery. However, its performance is inevitably limited by the gas mixing problem at the feed inlet position in adsorption columns, where discontinuity in the columns' axial concentration profiles disturbs the separation. Here, we developed a dynamic-feed DR-PSA (DF-DR-PSA) process to solve the mixing problem and obtain better separation performance by introducing multiple feed inlets along the column. The DF-DR-PSA process was demonstrated by enrichment methane (CH_4) from a binary gas mixture containing 2.4 mol.% CH_4 in nitrogen (N_2) using activated carbon material. Non-isothermal dynamic models were constructed to investigate the effects of operating parameters on the separation performance. Results showed the DF-DR-PSA process achieved both higher methane purity (53.5% versus 47.5%) and recovery (81.1% versus 72.2%) over the conventional DR-PSA process at the same energy consumption.

Topic heading: Separations: Materials, Devices and Processes

Keywords: gas separation, pressure swing adsorption (PSA), binary mixture, methane upgrading, numerical modelling

Introduction

Pressure swing adsorption (PSA) has been commonly investigated for gas separations, such as hydrogen purification[1], air separation[2], noble gases purification[3], separation of hydrogen isotopes[4], carbon dioxide (CO_2) capture[5] and methane (CH_4) upgrading[6]. Conventional PSA processes can be deployed in either stripping or enriching configurations[7], and they often produce only one high purity product by sacrificing its recovery due to their thermodynamic restrictions[8]. However, many gas separation processes often require both the enriched and lean gas streams to be relatively pure, i.e. targeting at high recoveries and purities simultaneously.

Dual-reflux PSA (DR-PSA) is a relatively new adsorption process proposed by Hirose[9] and Leavitt[10] in the 1990s. This process aims to overcome the process limitations of conventional PSA and achieve two high purity gas products (i.e. enriched and lean gas) simultaneously by combining two conventional PSA units using an intermediate feed position and a double reflux (i.e. light and heavy reflux) strategy, hence the name of DR-PSA. The schematic diagram of a DR-PSA process is presented in Fig. 1. This process consists of four fundamental steps: feed (FE), pressurization (PR), purge (PU) and blowdown (BD). Since the feed gas can be injected into the high pressure (PH) or the low pressure (PL) adsorption column, the pressure reversal can be accomplished by transferring gas between the enriching ends of both columns, which are rich in the heavy component (i.e., the more adsorbable, A) or the stripping ends that are rich in the light component (i.e., the less adsorbable, B). DR-PSA cycles have four basic configurations, i.e., DR-PL-A, DR-PH-A, DR-PL-B and DR-PH-B[7].

DR-PSA process has been widely investigated and successfully demonstrated to achieve both high purity light and heavy products simultaneously for various applications. The seminal experimental DR-PSA studies were conducted by Diagne et al.[8], in which zeolite MS 13X was used to separate CO_2 from the air with a PH-A configuration. Results showed that a feed gas stream with 20 mol.% CO_2 was enriched to 90 mol.% in the heavy product stream and stripped to 2.5 mol.% in the lean gas stream. Since then, several research[11-20] have proven that DR-PSA processes showed high separation performance for various applications, such as CO_2 capture, hydrocarbon upgrading and air separation. Bhatt et al.[21] performed a series of experiments for concentrating 5 mol.% CH_4 in N_2 using the DR-PH-A process and Norit RB1 activated carbon adsorbents. The CH_4 fraction in the enriched gas stream was 55.0 mol.% and the N_2 purity in the lean gas stream was 98.5 mol.%. Saleman et al.[22] reported the separation of CH_4 and N_2 mixtures with 2.4 – 49.6 mol.% CH_4 by a laboratory-scale DR-PL-A apparatus. The methane enrichment ratio could reach 21, upgrading CH_4 2.4 mol.% to 51.0 mol.%, however, the methane recovery was only 34.0%.

There have been several simulation investigations of DR-PSA processes, ranging from equilibrium-based analytical models[7,23-26] to rigorous non-isothermal numerical models[20,27-32]. Ebner and Ritter[23] established the first mathematical model based on equilibrium theory with a few simplified isotherm assumptions. They found that the DR-PSA process is feasible over a wide range of operation conditions, even with a pressure ratio as low as 1.1. Kearns and Webley[7] further advanced the equilibrium theory model and identified the nomenclature of four basic DR-PSA configurations. Bhatt et al.[21,33] demonstrated an isothermal model of the DR-PSA process to describe their experiments. Two separate interactions (i.e., heavy reflux interaction and pressure reverse interaction) were adopted to build the model on the Aspen Adsorption platform. This

model successfully predicted the product compositions observed in their reported experiments with deviations in the simulated CH_4 mole fractions ranging from -0.02 to 0.08 for the heavy product. Zhang et al.[27] developed a non-isothermal numerical model in the software package Aspen Adsorption and compared their results with experiments by Saleman et al.[22]. In this work, they used an ideal compressor during the constant pressure (FE and PU) steps, resulting in a high average material balance error of 8.6%; hence, the flow rate of light product and the concentrations of both product streams need to be corrected manually. Zou et al.[28] reported an advanced non-isothermal simulation model of the DR-PSA process and compared the predicted results with experimental data from McIntyre et al. [14] and Saleman et al.[22]. In this study, the isentropic compressor module and the PID controller module were applied to achieve the desired pressure profile, the standard deviation of the simulated predictions was 0.003 mol fraction in the ethane (C_2H_6) product stream compared with the experimental results from McIntyre et al. and 0.04 in the CH_4 product stream compared with experimental data from Saleman et al. May and co-workers[29-32] conducted a series of simulation-based studies of upgrading sub-quality natural gas by DR-PSA cycle, in which activated carbon, ionic liquidic zeolite (ILZ)[34] and ETS-4 were used as adsorbents successively.

The mixing problem, which manifests as a discontinuity in the columns' axial concentration profiles, has been reported by Diagne[12] and McIntyre[16], shown as Fig. 2 a and b. As illustrated in Fig. 2 a, the CO_2 concentration profiles are smooth on the upstream side of the feed inlet position. For instance, in the case of Z_F/L=0.6, the CO_2 molar fraction in the reflux flow is roughly 85%, dropping dramatically to around 20% after mixing with the feed gas (consisting of 20% CO_2). Fig. 2 b indicates a similar dip of ethane concentration (from approximately 57% to about 32%) just

after the feed position. Overall, this mixing problem particularly occurs at the feed inlet position in adsorption columns, caused by the concentration mismatch between the feed flow and upstream reflux flow, and can hamper the separation performance of the DR-PSA process. A range of researchers has focused on optimizing the feed position by matching the concentration of the feed gas and upstream reflux flow to minimize the effects of such concentration discontinuity problem[12,31,35]. Nevertheless, as the axial concentration profiles in the adsorption columns are time-dependent and the optimum feed position is also dynamic, this mixing problem is unavoidable for the DR-PSA process with a fixed feed location and feed concentration.

In this work, we proposed a dynamic feed (DF) DR-PSA process by introducing multiple feed positions along with the adsorption columns to a conventional DR-PSA process. This process is then demonstrated and compared with conventional DR-PSA processes using non-isothermal numerical simulations in Aspen Adsorption. A binary gas mixture of 2.4 mol.% CH_4 + 97.6 mol.% N_2 was used as the feed gas, a common vent stream in industrial liquefied natural gas (LNG) facilities. The robustness and reliability of the model were validated using the experimental data reported by Saleman et al.[22]. A sensitivity study was also conducted to investigate the impacts of the number of feed positions and the schedule of multiple feed steps. The outcome of this study will advance the knowledge of PSA and foster high-performance gas separations.

Simulation details

Model equations and description

The non-isothermal models of DR-PSA and DF-DR-PSA are constructed in Aspen Adsorption v10.0, a commercial software that can simulate the operation of dynamic adsorption cycles with rigorous pressure-flow (PF) networks and mass/energy balances. The governing equations and assumptions employed in this model are summarized in Table S1 in the supplementary information.

The partial differential equations used for the bed model are discretized using the Upwind Differencing Scheme 1 (UDS1), with 100 nodes distributed across a column; the Implicit Euler method is selected as the primary integration method; and the integration error tests only included states; the integrator configuration used in this simulation work is detailed in Table S2 in the supplementary information.

The flowsheet of DF-DR-PSA model

The flowsheet of the DF-DR-PSA process used to construct the non-isothermal model in Aspen Adsorption is shown in Fig. 3. The multiple positions of the feed inlet are modelled by segmenting the entire column into several column sections based on the simulated axial concentration profiles of the conventional DR-PSA process. The height of each column is specified in line with the entire column's length (H_b) and dimensionless feed inlet points (z_F). The minimum length of each column section is set at 0.049m (i.e., 5 grid nodes) to provide sufficient space between the inlet locations. The initialization of the simulation model is achieved by assigning the

concentration at all points in the PF network to be equal to that of the feed gas mixture. The temperature throughout the system was initially set to 293.15 K, the same as the environment temperature specified in simulations reported by Zhang et al.[27]. The initial pressures were set as 1.4 bar at the low-pressure side and 5 bar at the high-pressure side.

The model is configured to use the Norit RB3, a kind of activated carbon used in experiments of Saleman et al.[22]. Operational and bed model parameters, including the physical properties of the adsorbent used, are provided in Table 1.

The basic modules of the PF network are classified as follows:

1) Boundary streams: three boundary streams are named "Feed", "Heavy product", and "Light product" (as identified in Fig. 3), respectively, specified as non-reversible with constant pressure and temperature. During the PU/BD steps, the flowrates of boundary streams are set as zero. During the FE/PU steps, the molar flowrates of feed gas and heavy product streams are specified with a constant value, while the flowrate of the light product stream is controlled by a proportional–integral–derivative (PID) controller.

2) The PID controllers are applied to set the low and high pressures of the cycle. PID1 is introduced to determine the system's low pressure by controlling the volumetric flowrate through the compressor during the FE/PU steps and used to maintain a constant volumetric flowrate (5×10^{-5} m^3/s) during the PR/BD steps. PID2 is used to set the high pressure of the cycle by controlling the molar flowrate of the light product stream during the FE/PU steps.

3) Void tanks: two kinds of void tanks are employed in this model. One is used to represent the practical gas tank and acted as a buffer tank to avoid the pressure shock, set with a high volume value; the other one is served as a pressure node to match the so-called "P-F-P" connection requirement in Aspen Adsorption, specified with a little volume value.

4) Valves: valves are used to alter the flow direction and update steps of the DR-PSA cycle. In Aspen Adsorption, valves could be specified as four statuses: 0, fully closed; 1, fully open; 2, constant C_V; 3, constant molar flowrate. In this model, the valves are specified according to the flow status of different streams during the cycle, for instance, V_{LR1} and V_{LR2} would be switched between 0, 2 and 3 at different steps.

Model validation

This non-isothermal numerical model of DR-PSA was validated against the experimental results from Saleman et al. [22], consisting of 24 runs of various feed compositions (2.4 – 49.6 mol.% CH_4 balanced with N_2) and operating parameters (H/F ratio and R_L, i.e., the heavy to feed flow ratio and the light reflux flowrate). The comparison of the simulated and experimental cycle-averaged concentration of methane in both light (y_L) and heavy product (y_H) streams at the cyclic steady state (CSS) are shown in Fig. 4. In this simulation, the criterion for judging whether the simulation had achieved the CSS was built on the error of the total loading and solid-phase temperature between the two successive cycles. The simulation will be considered at CSS when the error is lower than the pre-set tolerance, which is 10^{-5} in this model. At CSS, the average overall material balance error is -0.3%, while the average CH_4 and N_2 component material balance error is 3.5% and -0.7%, respectively, comparable in magnitude to those of other DR-PSA models reported in

the open literature[27,29,32,33]. The RMSD (Root Mean Squared Deviation) evaluates the average error between the experimental and simulated results. The RMSD values for y_H and y_L are 0.021 and 0.007, respectively. Hence, this model accurately predicts the performance of the DR-PSA apparatus and can be exploited for further study.

Results and discussion

This rigorous non-isothermal model was used to numerically study the separation performance of the DF-DR-PSA process for concentrating dilute methane gas mixture (containing 2.4 mol.% methane) under various operating conditions.

Determination of dynamic-feed range

The concentration discontinuity in the axial profiles for conventional DR-PSA processes, considered as the "mixing problem" within the column, is due to the mixing of the feed stream and the upstream reflux flow[12], as shown in Fig. 5 a. Such discontinuity and sharp concentration changes cause significant perturbation to the column and hamper the separation performance. Previous studies[12,31,35] optimized the feed position via matching the concentration between the upstream reflux flow and the feed mixture. However, as illustrated in Fig. 5 a, the column's adsorption front is time-dependent during the feed step, moving from the stripping end to the enriching end, which means that there are varying optimum feed inlet positions at different times. Hence, the dynamic-feed strategy was exploited to solve the so-called "perturbation" problem. In Fig. 5, the black dashed line indicates a methane fraction of 2.4 mol.%, i.e., the feed methane concentration. The dynamic-feed range is determined by the two interactions of the dashed line

and axial concentration distribution curves at the start (0 s) and the end (120 s) of the feed step, along which the dynamic-feed strategy could be adopted, as indicated in Fig. 5 b.

Sensitivity study of the number of feed points

The switch policy of feed position was determined based on the simulated axial concentration profiles of the DR-PSA configuration. Two methods were implemented to optimize the dynamic feeding policy for the DF-DR-PSA process:

1) Dividing the feed step averagely into multiple sub-steps and locating the optimum feed inlet position for each sub-step, i.e., the uniform time method;

2) Dividing the dynamic-feed range equally into multiple column sections with identified feed locations and finding the time points at which the upstream reflux concentration is equal to the feed concentration, i.e., the uniform space method.

The impact of feed inlet points numbers (n) on the separation performance was investigated, as shown in Fig. 6. Results indicate that the DF-DR-PSA process, introducing either of the mentioned approaches, can achieve better separation performance than the conventional DR-PSA process. As the feed inlet positions increase from 3 to 8, the methane purity (y_H) and recovery increased by 2.7 mol.% and 5.8%, respectively. The cycles generally perform better when exploiting the uniform space method in terms of product purity, whereas for the methane recovery, there is no significant difference between these two methods.

Fig. 7 a and Fig. 7 b respectively show methane axial concentration profiles of two methods, case (a) using the uniform time strategy, whereas case (b) with the uniform space method, both runs

had eight feed inlet positions. As illustrated in Fig. 7, compared with the fraction profiles in Fig. 5, the axial concentration distribution curves of the DF-DR-PSA process are smoother and have no significant perturbation at each feed point, indicating that the dynamic-feed strategy is capable of solving the mixing problem. It is noteworthy that the concentration profile using the uniform space method is generally smoother than the one using the uniform time method, which explains why the uniform space method performs better. Therefore, the uniform space method was adopted to achieve the dynamic-feed target in the following study due to its better separation performance. The independence of computed results on the mesh division of adsorption column sections was investigated to avoid the performance improvements was driven by different meshing between the DR-PSA and DF-DR-PSA configurations, as detailed in Table S3 and Fig. S1 in the supplementary information.

Parametric study of the DF-DR-PSA process

The purities and recoveries of the conventional DR-PSA used in this section are selected at the optimum feed position. The complete results of purity and recovery at different feed positions under varying operating conditions obtained by the conventional DR-PSA process are plotted as Fig. S2 – S4 in the supplementary information. The parameters H/F ratio, light reflux flowrate (R_L), and feed step time ($t_{FE/PU}$), which have been proven to significantly impact the separation performance of DR-PSA cycles, were chosen to conduct the parametric study in this work.

Effect of the H/F ratio

The theoretical boundary values of y_H and y_L are a function of the ratio of heavy product flowrate to feed flowrate (H/F) and the feed gas concentration (y_F) and shown in Eq. 1 and Eq. 2.

$$y_H \begin{cases} \leq 1, & \text{if } H/F \leq y_F \\ \leq \frac{y_F}{\frac{H}{F}}, & \text{if } H/F \geq y_F \end{cases} \quad \text{Eq. 1}$$

$$y_L \begin{cases} \geq \frac{y_F - \frac{H}{F}}{1 - \frac{H}{F}}, & \text{if } H/F \leq y_F \\ \geq 0, & \text{if } H/F \geq y_F \end{cases} \quad \text{Eq. 2}$$

As the feed flowrate is constant (*F*=1.25 SLPM) in this study, the *H*/*F* ratio can be adjusted by changing the heavy product flowrate. The separation performance of conventional DR-PSA and DF-DR-PSA processes is shown in Fig. 8 for relevant *H*/*F* ratios. According to Eq. 1 and Eq. 2, the perfect separation performance can only be obtained when *H*/*F* is equal to y_F for an ideal DR-PSA process, which is impractical in reality. The separation performance can be biased towards higher purity or recovery by varying the H/F ratio for an actual cycle. Fig. 8 shows an increase in purity and decrease in recovery with decreasing *H*/*F* ratio, which applies to both processes. Numerical simulation results in the figure show that the performance of the DF-DR-PSA cycle, in terms of both purity and recovery, are generally better than that of the conventional DR-PSA process. The DF-DR-PSA process can obtain both higher purity (53.5% versus 47.5%) and recovery (81.1% versus 72.2%) compared to the conventional DR-PSA process.

A Pareto plot of methane recovery versus product purity is shown in Fig. 9 to illustrate their competitive relationship. The arrow indicates the direction of decreasing *H*/*F* ratios. The purity is increased at the expense of methane recovery, revealing the usual trade-off between product purity and recovery. The DF-DR-PSA shows distinct superiority over the conventional DR-PSA, especially when *H*/*F* is around 0.024, which is the theoretically ideal *H*/*F* value as discussed.

Effect of light reflux flowrate

Reflux flowrate is another crucial operating parameter which has significant impacts on separation performance. Since the heavy reflux flowrate (R_H) is coupled to the light reflux flowrate (R_L), in this study, the light reflux flowrate was specified as flow-controlled and the heavy reflux flowrate was set as pressure-controlled. The H/F ratio was set constant at 0.042, and the feed step duration is 120s. The simulated purity and recovery are plotted in Fig. 10 as a function of R_L. As shown in Fig. 10, for the conventional DR-PSA process, product purity y_H first increases when the light reflux flow raises from 0.8 to 2.0 SLPM, reaching a maximum value when the R_L is around 2 SLPM. After that, the product purity declines gradually with a further increase of R_L. The optimum R_L value is between 2 to 2.5 SLPM to obtain the best recovery. A similar trend can be observed when altering R_L for the DF-DR-PSA process. The optimum R_L is approximately 2.8 SLPM, corresponding to the best purity and about 2.3 SLPM for the best recovery. It is worthy to note that there is a minimum R_L value below which the purity of the DF-DR-PSA process is even lower than that of conventional DR-PSA configuration. When the R_L value is small, there is insufficient light purge gas to clean the adsorbent. Additionally, the dynamic-feed range is too narrow to set enough feed positions. Hence, a light reflux flowrate above the threshold value is necessary to ensure adequate desorption of CH_4 from the low-pressure column and guarantee a sufficiently wide dynamic-feed range for the DF-DR-PSA cycle.

Effect of feed step duration

Two steps are involved in the DR-PSA and DF-DR-PSA processes:

- FE/PU step for adsorption in the high-pressure column and desorption in the low-pressure column;

- PR/BD step duration for pressure inversion.

FE/PU step duration is crucial for optimizing the adsorption front position to avoid the breakthrough and maximize CH_4 productivity. A series of strep durations including 80s, 100s, 120s, 140s and 160s are investigated to optimize the step duration, as illustrated in Fig. 11. Fig. 11 a shows that the DF-DR-PSA cycle reaches the maximum y_H value of 44.5 mol.% at 100 s. The deviations between the two processes reduce with the decreasing feed step time, which is due to the reduction of $t_{FE/PU}$ will shorten the dynamic-feed range. Fig. 11 b shows that both the methane purity and recovery using the DF-DR-PSA process are superior to the conventional DR-PSA process. For instance, when the $t_{FE/PU}$ is 100 s, the purity and recovery are improved by roughly 2% and 5%, respectively.

Bed productivity is another indicator to evaluate the performance of a process, which is defined by the amount of product per unit amount of adsorbent per unit time, as illustrated in Eq. 3.

$$Prod_{\mathrm{CH_4}} = \frac{y_H \cdot H \cdot t_{FE/PU}}{(t_{FE/PU}+t_{PR/BD}) \cdot m_{ads}} \quad \text{Eq. 3}$$

Here, H is the flowrate of the heavy product stream, and m_{ads} denotes the mass of the adsorbent.

In Fig. 12, bed productivity is shown at varying feed step durations $t_{FE/PU}$ with constant light reflux flowrate R_L and H/F ratio. For the DF-DR-PSA process, productivity ranges from (0.036 to 0.046) mol CH_4 kg^{-1} hr^{-1}, which is higher than that of the conventional DR-PSA cycle, whose productivity ranges from 0.034 to 0.043 mol CH_4 kg^{-1} hr^{-1}. The DF-DR-PSA cycle achieves higher productivity due to its better product purity results than the conventional DR-PSA configuration. The productivity reduces with decreasing values of $t_{FE/PU}$ as the percentage of gas production time to

the total cycle time decreases. However, such lower $t_{FE/PU}$ values also lead to higher product purity, revealing the general trade-off between purity and productivity.

Conclusions

In this work, we proposed and demonstrated a novel dynamic-feed DR-PSA process for the enrichment of dilute CH_4 (2.4 mol.%) from its mixture with N_2. A performance comparison of the conventional DR-PSA and DF-DR-PSA processes were conducted with numerical simulation using Norit RB3 activated carbon adsorbents. The effects of heavy product/feed flowrate (*H*/*F*) ratio, light reflux flowrate (R_L) and step durations ($t_{FE/PU}$) on the process performance of both two processes were investigated. The sensitivity study illustrated that both higher purity and recovery could be achieved when more feed inlet positions were set along with the columns. Simulated results showed that the DF-DR-PSA cycle performed better than the conventional DR-PSA cycle in terms of product purity, recovery and productivity. The comparison of methane concentration profiles in the adsorption column during the feed step suggested that the mixing problem of conventional DR-PSA processes could be practically solved by introducing the dynamic-feed strategy. Results showed the DF-DR-PSA process achieved both higher methane purity (53.5% versus 47.5%) and recovery (81.1% versus 72.2%) over the conventional DR-PSA process at the same energy consumption.

Acknowledgements

This project is funded by the Australia Research Council (DP190100983). Y. Guo would like to thank J. Yu for providing research facilities to run part of simulations in this work.

Glossary

PSA Cycles and Steps:

BD	Blowdown step
DR-PSA	Dual Reflux Pressure Swing Adsorption
DF-DR-PSA	Dynamic-feed Dual Reflux Pressure Swing Adsorption
FE	Feed step (desorption)
PR	Pressurization step
PU	Purge step (adsorption)

Pressure-Flow Network Components in Simulation

PID1	PID controller for the compressor
PID2	PID controller for the Light product valve
VF	System feed valve
VF1-n	Column 1 feed valve at feed point *n*
VF2-n	Column 2 feed valve at feed point *n*
VH	System heavy product valve
VH1	Column 1 heavy product valve
VH2	Column 2 heavy product valve
VHR1	Column 1 heavy reflux valve
VHR2	Column 2 heavy reflux valve
VL	System light product valve
VLR1	Column 1 light reflux valve
VLR2	Column 2 light reflux valve

Literature cited

1. Silva B, Solomon I, Ribeiro AM, Lee UH, Hwang YK, Chang JS, Loureiro JM, Rodrigues AE. H2 purification by pressure swing adsorption using CuBTC. *Separation and Purification Technology.* 2013;118:744-756.

2. Xu M, Wu H-C, Lin YS, Deng S. Simulation and optimization of pressure swing adsorption process for high-temperature air separation by perovskite sorbents. *Chemical Engineering Journal.* 2018;354:62-74.

3. Jin X, Malek A, Farooq S. Production of Argon from an Oxygen−Argon Mixture by Pressure Swing Adsorption. *Industrial & Engineering Chemistry Research.* 2006;45(16):5775-5787.

4. Si Y, He X, Jiang J, Duan Z, Wang W, Yuan D. Highly effective H2/D2 separation in a stable Cu-based metal-organic framework. *Nano Research.* 2019.

5. Xu M, Chen S, Seo D-K, Deng S. Evaluation and optimization of VPSA processes with nanostructured zeolite NaX for post-combustion CO2 capture. *Chemical Engineering Journal.* 2019;371:693-705.

6. Hu G, Zhao Q, Tao L, Xiao P, Webley PA, Li KG. Enrichment of low grade CH4 from N2/CH4 mixtures using vacuum swing adsorption with activated carbon. *Chemical Engineering Science.* 2021;229.

7. Kearns DT, Webley PA. Modelling and evaluation of dual-reflux pressure swing adsorption cycles: Part I. Mathematical models. *Chemical Engineering Science.* 2006;61(22):7223-7233.

8. Diagne D, Goto M, Hirose T. New Psa Process with Intermediate Feed Inlet Position Operated with Dual Refluxes - Application to Carbon-Dioxide Removal and Enrichment. *Journal of Chemical Engineering of Japan.* Feb 1994;27(1):85-89.

9. Hirose T. A simple design method of a new PSA process consisting of both rectifying and stripping sections. Paper presented at: Proceedings of the 2nd China-Japan-USA Symposium on Adsorption1991.

10. Leavitt FW. Duplex adsorption process: US Patent 5,085,674; 1992.

11. Diagne D, Goto M, Hirose T. Experimental-Study of Simultaneous Removal and Concentration of CO2 by an Improved Pressure Swing Adsorption Process. *Energ Convers Manage.* Jun-Sep 1995;36(6-9):431-434.

12. Diagne D, Goto M, Hirose T. Parametric Studies on CO2 Separation and Recovery by a Dual Reflux Psa Process Consisting of Both Rectifying and Stripping Sections. *Industrial & Engineering Chemistry Research.* Sep 1995;34(9):3083-3089.

13. Dong F, Lou H, Goto M, Hirose T. A new PSA process as an extension of the Petlyuk distillation concept. *Separation and Purification Technology.* 1999;15(1):31-40.

14. McIntyre JA, Holland CE, Ritter JA. High Enrichment and Recovery of Dilute Hydrocarbons by Dual-Reflux Pressure-Swing Adsorption. *Industrial & Engineering Chemistry Research.* 2002;41(14):3499-3504.

15. Wakasugi R, Kodama A, Goto M, Hirose T. Dual Reflux PSA Process Applied to VOC Recovery as Liquid Condensate. *Adsorption.* 2005;11(S1):561-566.

16. McIntyre JA, Ebner AD, Ritter JA. Experimental Study of a Dual Reflux Enriching Pressure Swing Adsorption Process for Concentrating Dilute Feed Streams. *Industrial & Engineering Chemistry Research.* 2010;49(4):1848-1858.

17. Li D, Zhou Y, Shen Y, Sun W, Fu Q, Yan H, Zhang D. Experiment and simulation for separating CO2/N2 by dual-reflux pressure swing adsorption process. *Chemical Engineering Journal.* 2016;297:315-324.

18. May EF, Zhang Y, Saleman TLH, Xiao G, Li G, Young BR. Demonstration and optimisation of the four Dual-Reflux Pressure Swing Adsorption configurations. *Separation and Purification Technology.* 2017;177:161-175.

19. Shen Y, Zhou Y, Li D, Fu Q, Zhang D, Na P. Dual-reflux pressure swing adsorption process for carbon dioxide capture from dry flue gas. *International Journal of Greenhouse Gas Control.* 2017;65:55-64.

20. Tian C, Fu Q, Ding Z, Han Z, Zhang D. Experiment and simulation study of a dual-reflux pressure swing adsorption process for separating N2/O2. *Separation and Purification Technology.* 2017;189:54-65.

21. Bhatt TS, Sliepcevich A, Storti G, Rota R. Experimental and Modeling Analysis of Dual-Reflux Pressure Swing Adsorption Process. *Industrial & Engineering Chemistry Research.* 2014;53(34):13448-13458.

22. Saleman TL, Li G, Rufford TE, Stanwix PL, Chan KI, Huang SH, May EF. Capture of low grade methane from nitrogen gas using dual-reflux pressure swing adsorption. *Chemical Engineering Journal.* Dec 1 2015;281:739-748.

23. Ebner AD, Ritter JA. Equilibrium theory analysis of dual reflux PSA for separation of a binary mixture. *AIChE Journal.* 2004;50(10):2418-2429.

24. Bhatt TS, Storti G, Rota R. Optimal design of dual-reflux pressure swing adsorption units via equilibrium theory. *Chemical Engineering Science.* 2013;102:42-55.

25. Rossi E, Storti G, Rota R. Influence of the main operating parameters on the DRPSA process design based on the equilibrium theory. *Adsorption.* 2020.

26. Bhatt TS, Storti G, Denayer JFM, Rota R. Equilibrium Theory-Based Assessment of Dual-Reflux Pressure Swing Adsorption Cycles That Utilize Light Gas for Pressure Swing. *Industrial & Engineering Chemistry Research.* 2018;58(1):350-365.

27. Zhang Y, Saleman TLH, Li G, Xiao G, Young BR, May EF. Non-isothermal numerical simulations of dual reflux pressure swing adsorption cycles for separating N 2 + CH 4. *Chemical Engineering Journal.* 2016;292:366-381.

28. Zou Y, Xiao G, Li G, Lu W, May EF. Advanced non-isothermal dynamic simulations of dual reflux pressure swing adsorption cycles. *Chemical Engineering Research and Design.* 2017;126:76-88.

29. Weh R, Xiao G, Islam MA, May EF. Upgrading sub-quality natural gas by dual reflux-pressure swing adsorption using activated carbon and ionic liquidic zeolite. *Chemical Engineering Journal.* 2019.

30. Xiao G, Saleman TL, Zou Y, Li G, May EF. Nitrogen rejection from methane using dual-reflux pressure swing adsorption with a kinetically-selective adsorbent. *Chemical Engineering Journal.* 2019;372:1038-1046.

31. Lu W, Xiao G, Weh R, May EF. Rejecting N2 from natural gas by dual reflux pressure swing adsorption with activated carbon. *Journal of Natural Gas Science and Engineering.* 2020;81.

32. Weh R, Xiao G, Islam MA, May EF. Nitrogen rejection from natural gas by dual reflux-pressure swing adsorption using activated carbon and ionic liquidic zeolite. *Separation and Purification Technology.* 2020;235.

33. Bhatt TS, Storti G, Rota R. Detailed simulation of dual-reflux pressure swing adsorption process. *Chemical Engineering Science.* 2015;122:34-52.

34. Li G, May EF, Webley PA, Huang SH-w, Chan KI. Method for gas separation. USA2017.

35. Diagne D, Goto M, Hirose T. Numerical analysis of a dual refluxed PSA process during simultaneous removal and concentration of carbon dioxide dilute gas from air. *J Chem Technol Biot.* Jan 1996;65(1):29-38.

List of Figure Captions

Fig. 1 Schematic diagram of a complete DR-PSA cycle in four basic configurations: feed to high pressure (PH) or low pressure (PL) adsorption column, and heavy (A) or light (B) gases for pressure inversion.

Fig. 2 Mixing problem reported by Diagne (a) and McIntyre (b). The red line indicates the sharp concentration increase, and the blue line exhibits a significant concentration decrease. (a) CO_2 concentration profiles at various values of the feed inlet position, adapted with permission from (Ref. 12). Copyright (1995) American Chemical Society. (b) Ethane concentration profiles in the column at the end of the heavy reflux step, adapted with permission from (Ref. 16). Copyright (2010) American Chemical Society.

Fig. 3 Process flowsheet diagram for the numerical model to simulate the conventional DR-PSA process and the DF-DR-PSA process. The number of adsorption columns (N+1) is determined by the number of feed positions (n).

Fig. 4 Deviations of y_{sim} predicted in the numerical simulation from the corresponding values y_{exp} measured in experiments [22].

Fig. 5. (a) Axial concentration distributions in the conventional DR-PSA column at the time point of 0, 20, 40, 60, 80, 100 and 120 s during the feed step (operating parameters are specified as R_L=2.302, H/F≈0.042, and $t_{FE/PU}$=120 s). z is the dimensionless axial position along the column, z=0 is the enriching end, z=1 is the stripping end, feed position is z_F=0.7. (b) Enlarged diagram of the dynamic feed range.

Fig. 6 The purity (a) and recovery (b) of methane by DF-DR-PSA cycles as a function of n (the number of feed inlet points). The operating parameters are R_L=2.302, H/F≈0.042, and $t_{FE/PU}$=120s). The dashed line represents the result using the conventional DR-PSA process under the same operating conditions.

Fig. 7 Axial concentration distributions in the DF-DR-PSA column at the time point of 0, 20, 40, 60, 80, 100 and 120 during the feed step by the uniform time method (a) and the uniform space method (b). The operating parameters are R_L=2.302, H/F≈0.042, and $t_{FE/PU}$=120 s.

Fig. 8 The effect of H/F ratios on the purity (a) and recovery (b) of methane at constant $t_{FE/PU}$=120 s and R_L=2.302 SLPM. The arrows indicate the direction in which the H/F ratio should be varied to bias the separation performance favouring the purity or the recovery.

Fig. 9 The correlation between methane recovery and heavy product purity.

Fig. 10 The purity (a) and recovery (b) of methane by two kinds of cycles as a function of the R_L. The results of the conventional DR-PSA process are picked from the optimum fixed feed position.

Fig. 11 The purity (a) and recovery (b) of methane by two processes as a function of the $t_{FE/PU}$ at constant R_L=2.302 SLPM and H/F=0.042.

Fig. 12 The productivity of methane by two kinds of cycles as a function of the $t_{FE/PU}$ at constant R_L=2.302 SLPM and H/F=0.042.

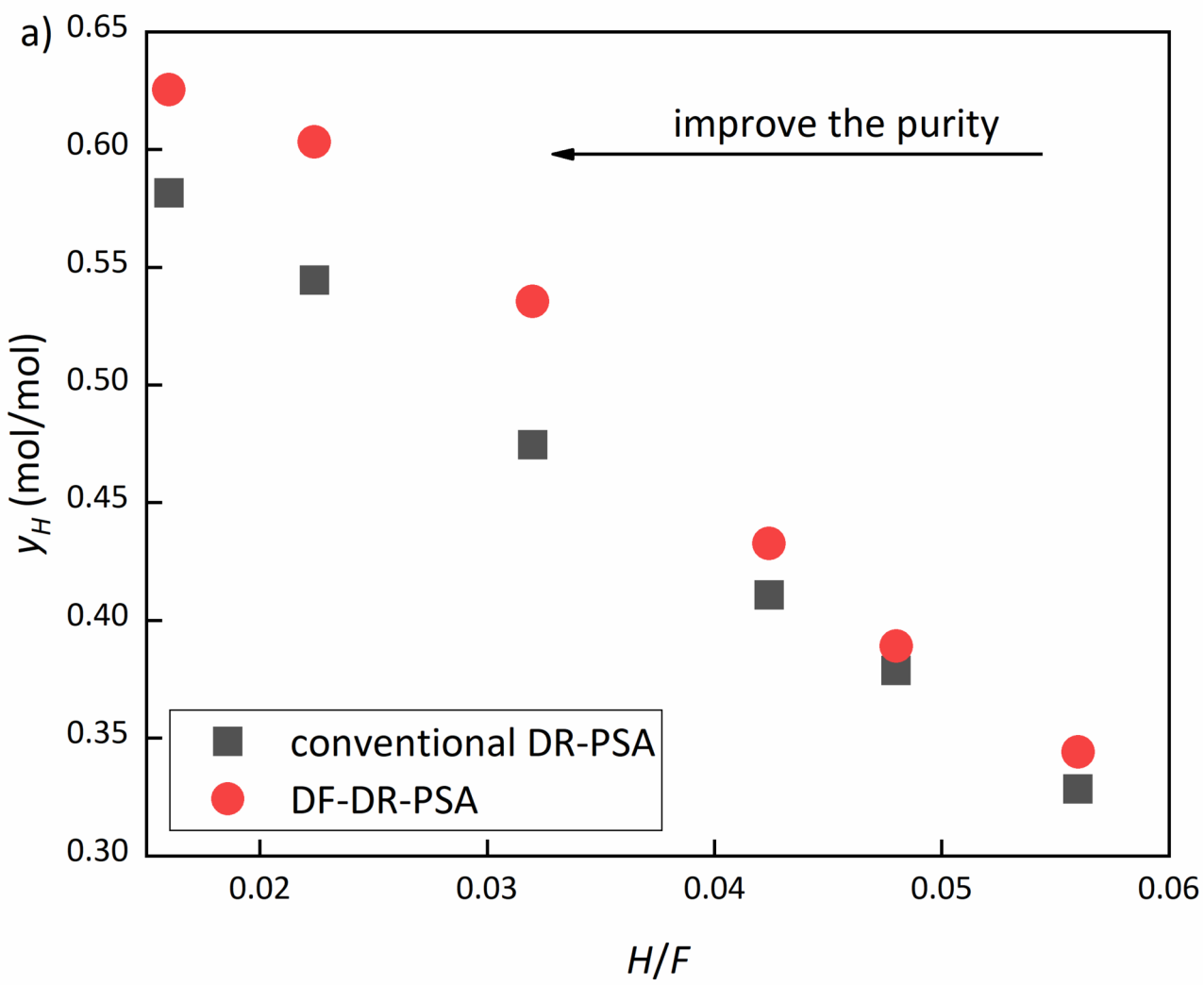

AIC_17390_fig.8a.tif

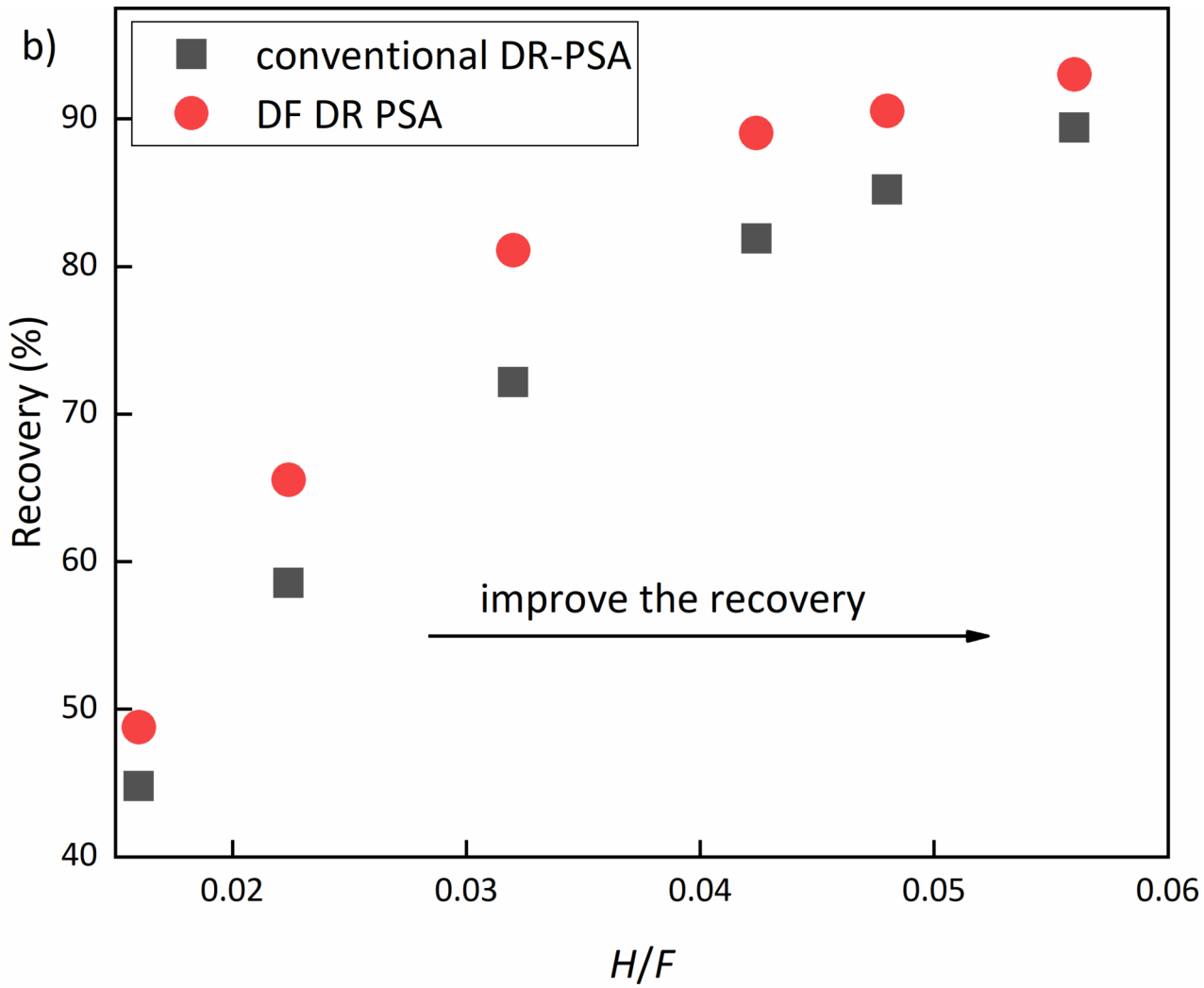

AIC_17390_fig.8b.tif

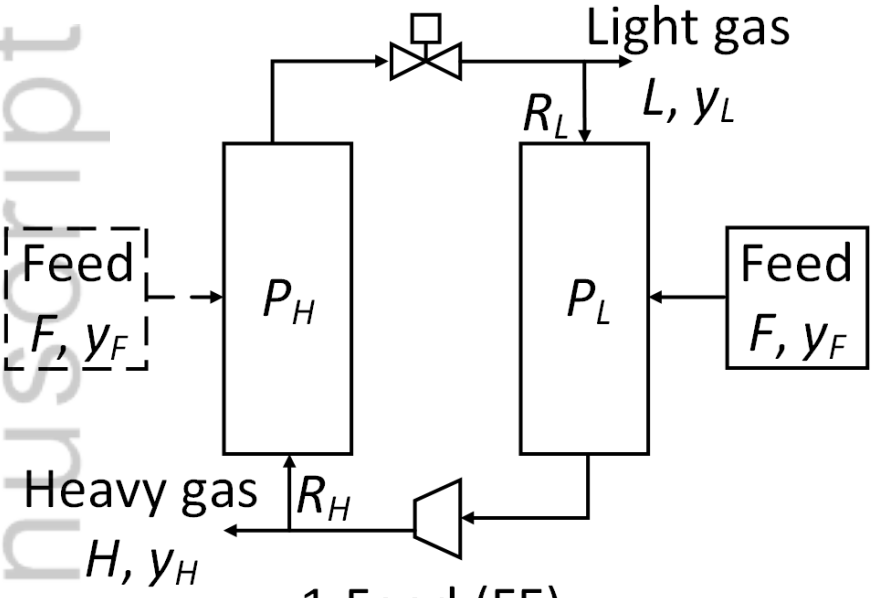

1.Feed (FE)

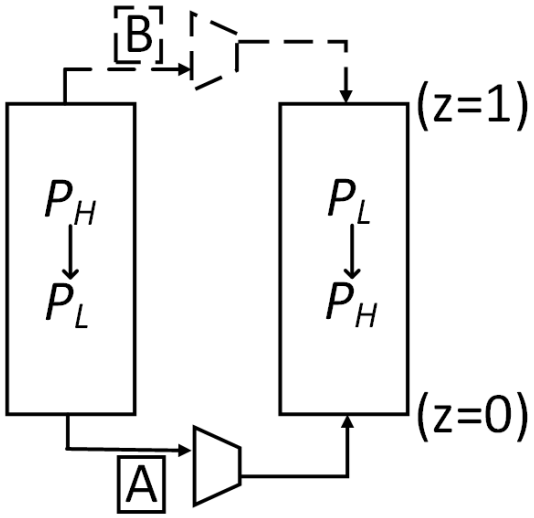

2.Pressurization (PR)

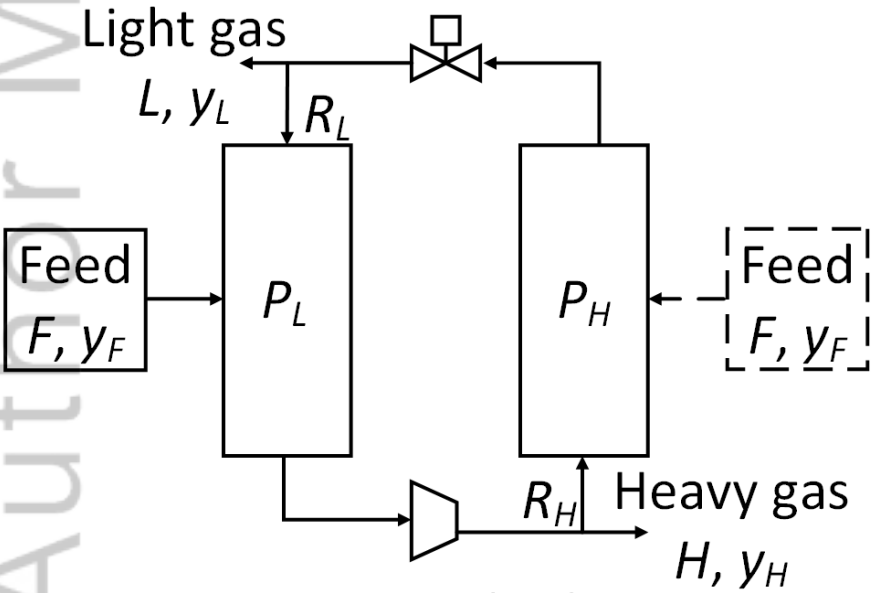

3.Purge (PU)

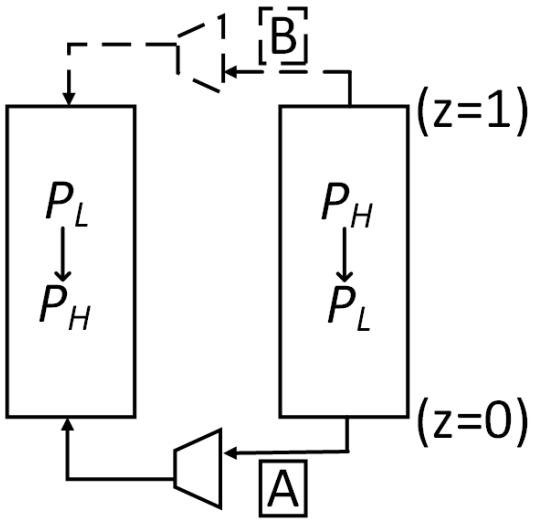

4.Blowdown (BD)

AIC_17390_Fig.1.tif

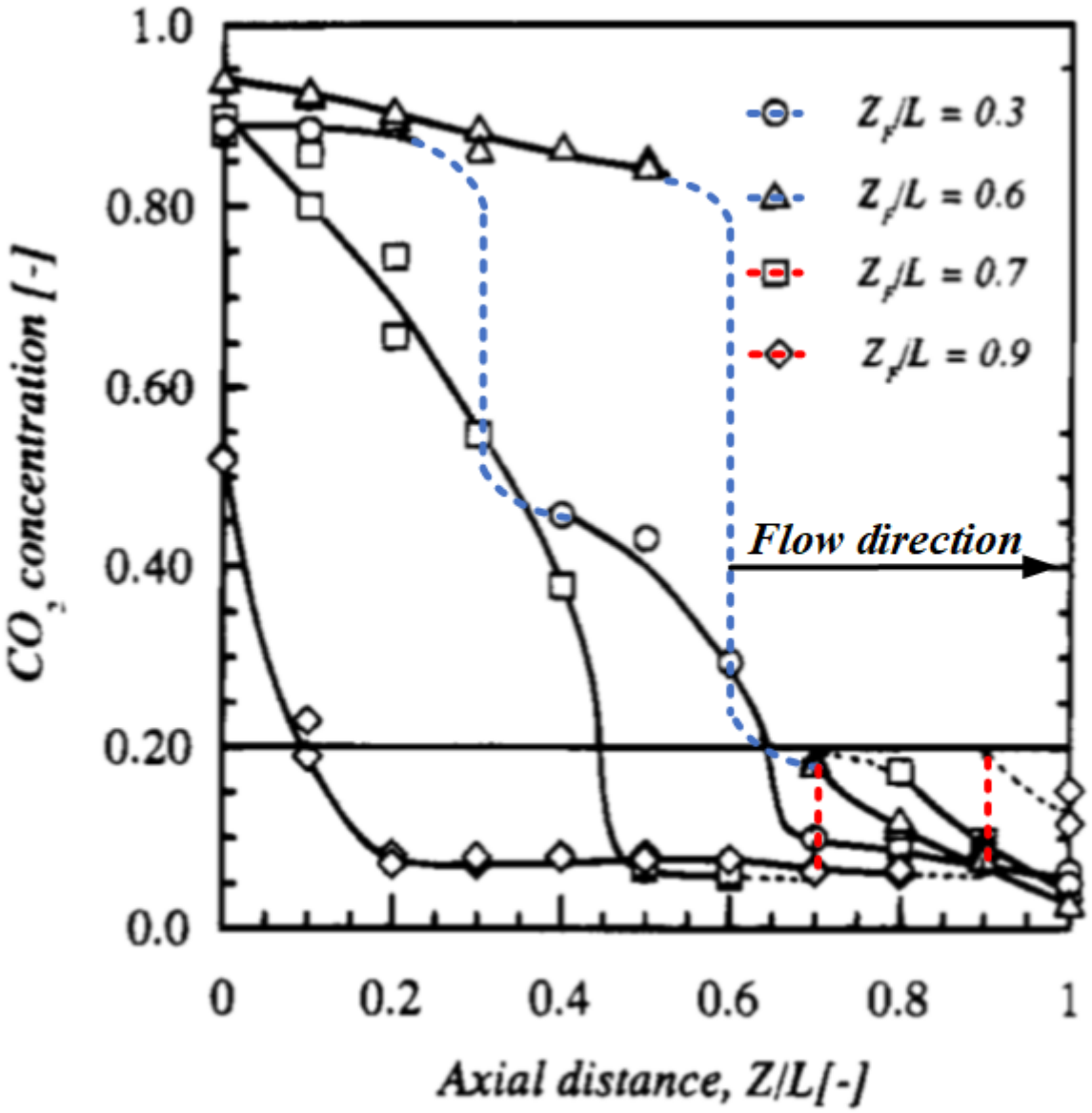

AIC_17390_Fig.2 a.tif

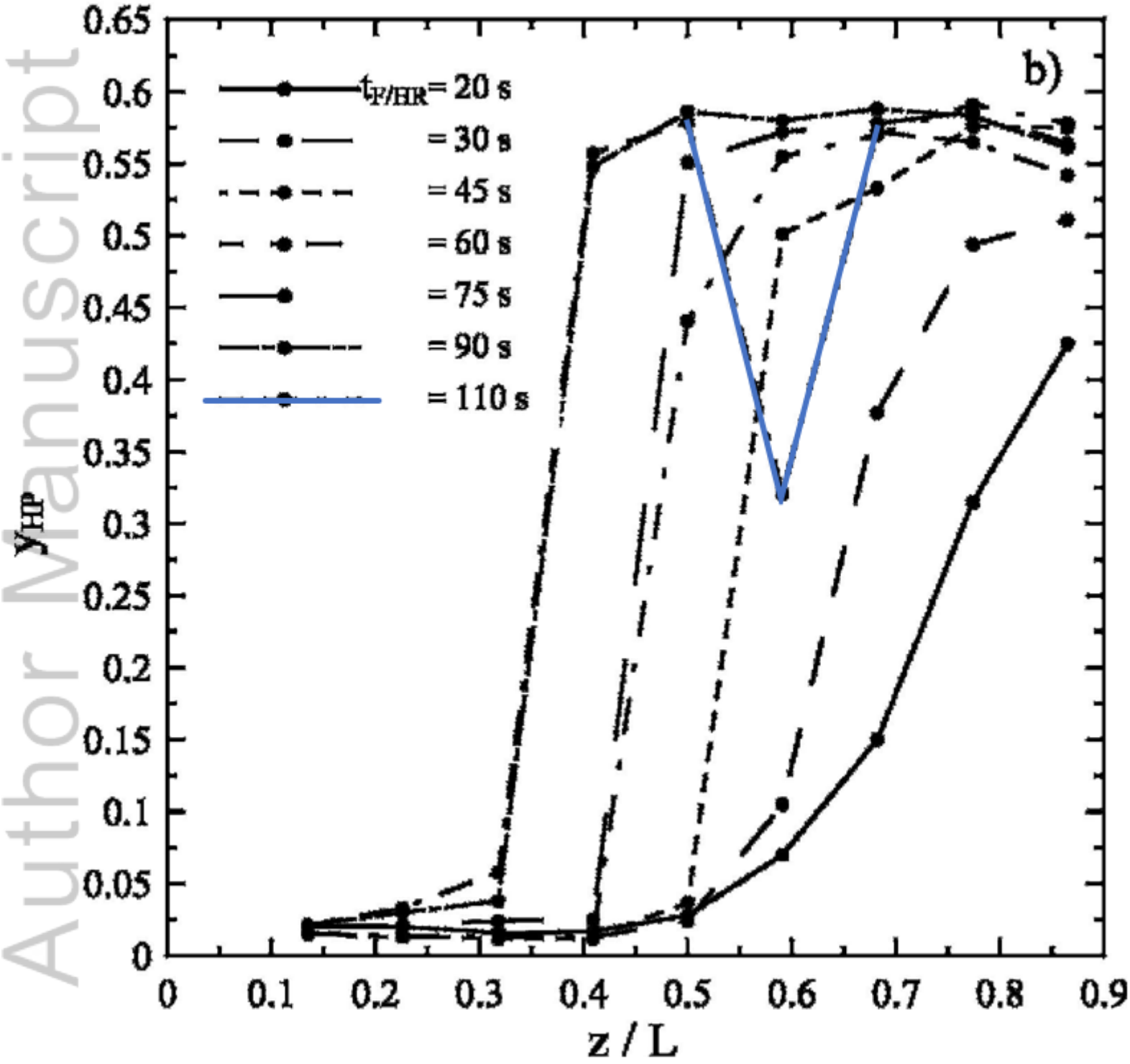

AIC_17390_Fig.2 b.tif

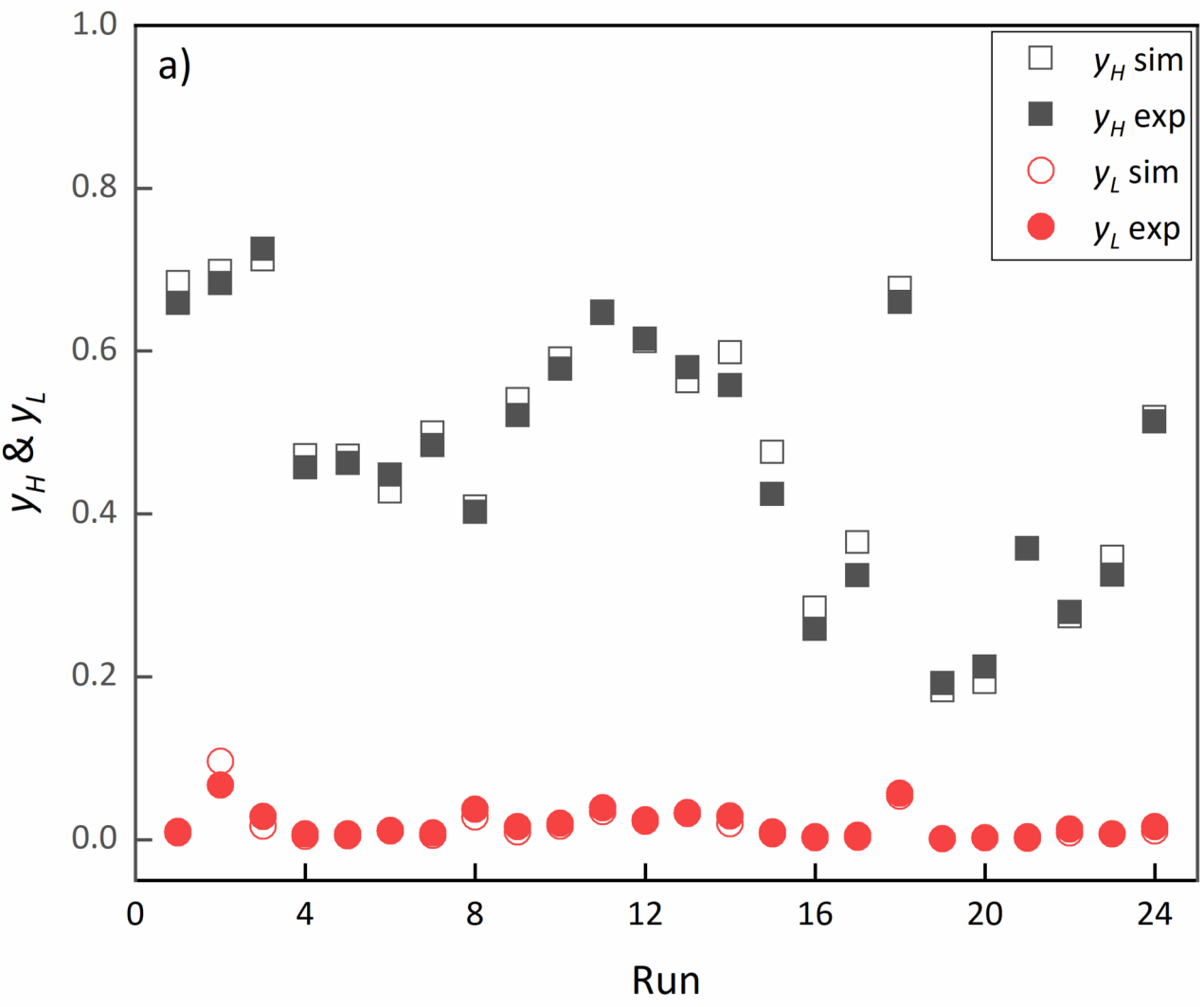

AIC_17390_Fig.4a.tif

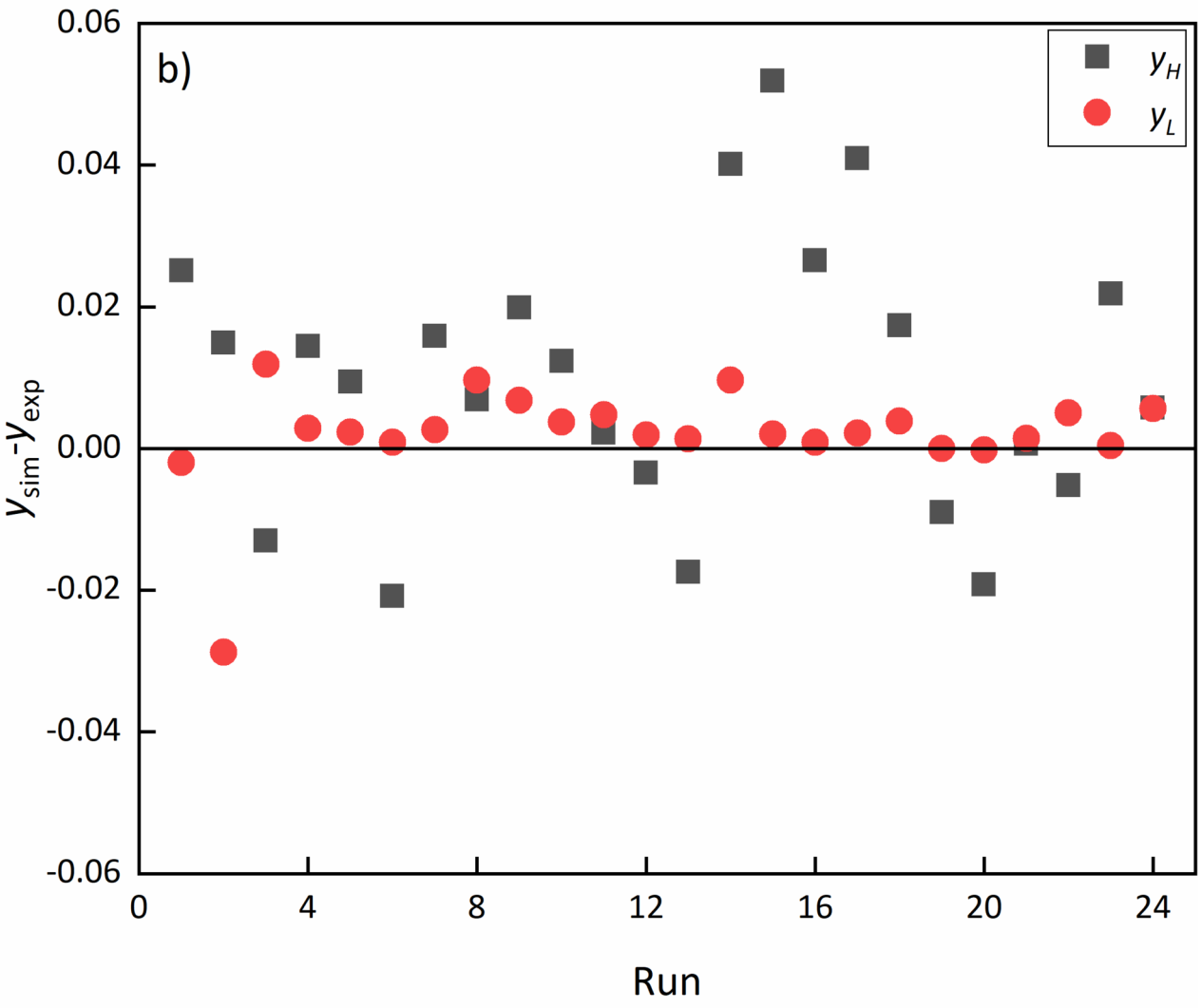

AIC_17390_Fig.4b.tif

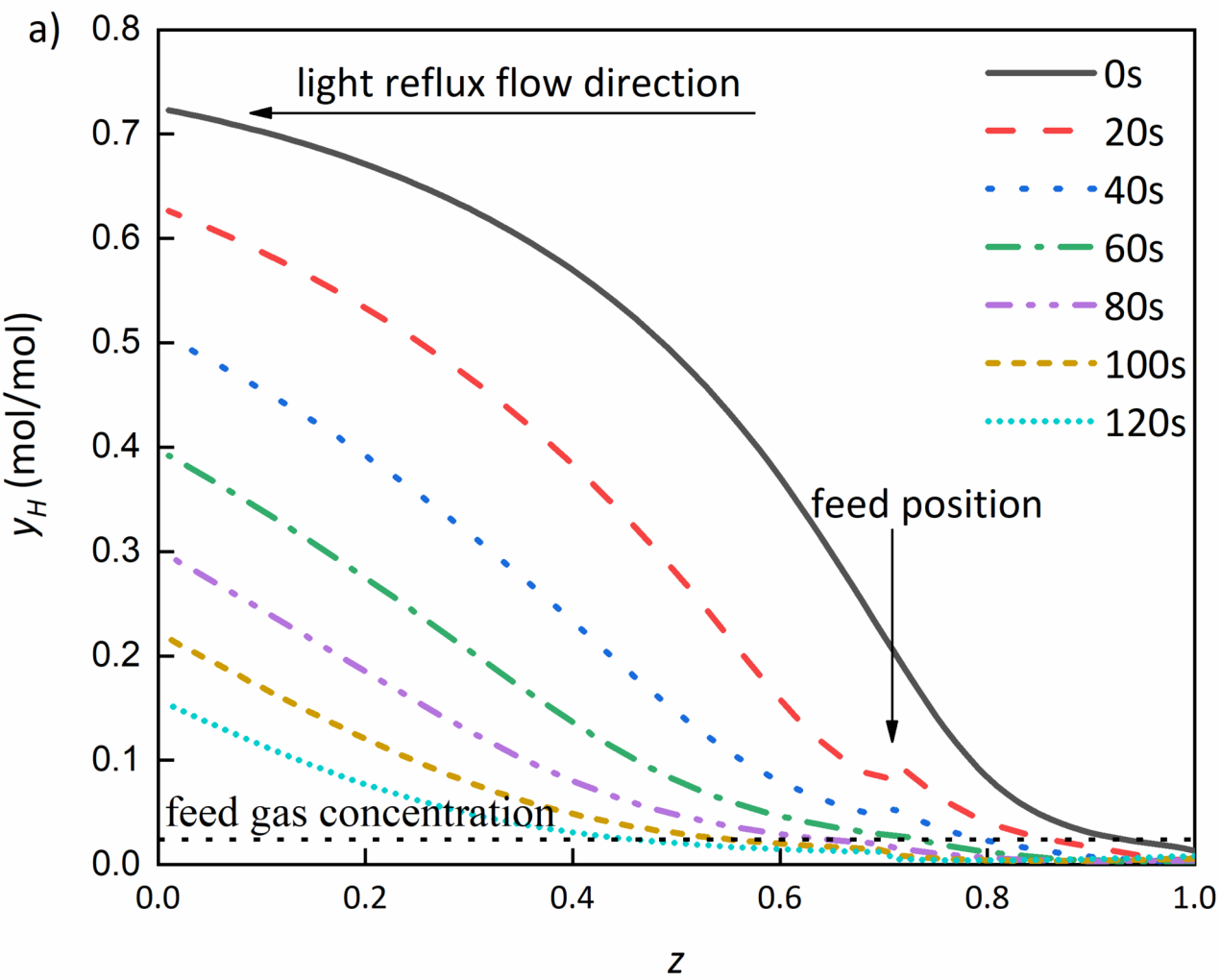

AIC_17390_Fig.5a.tif

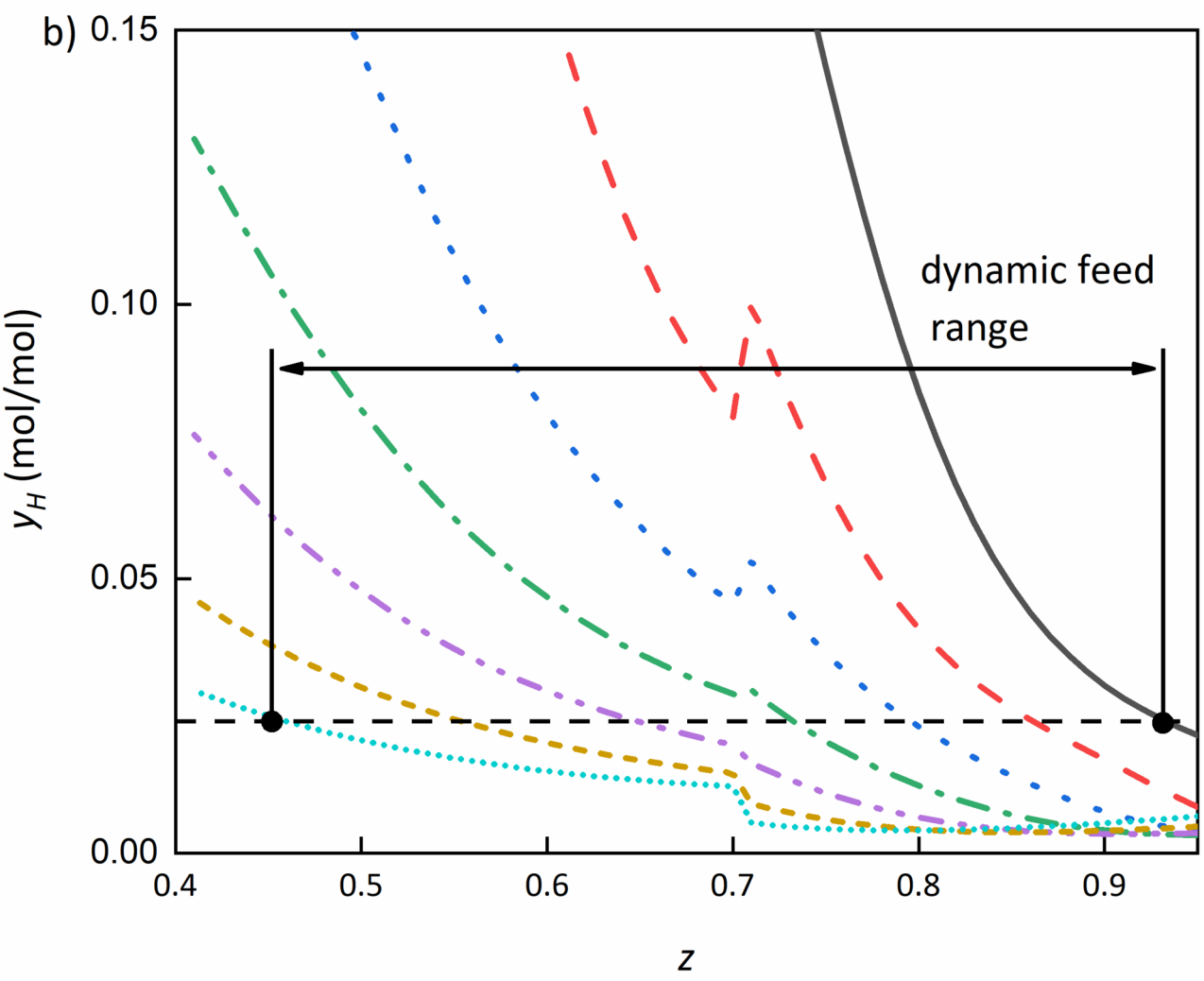

AIC_17390_Fig.5b.tif

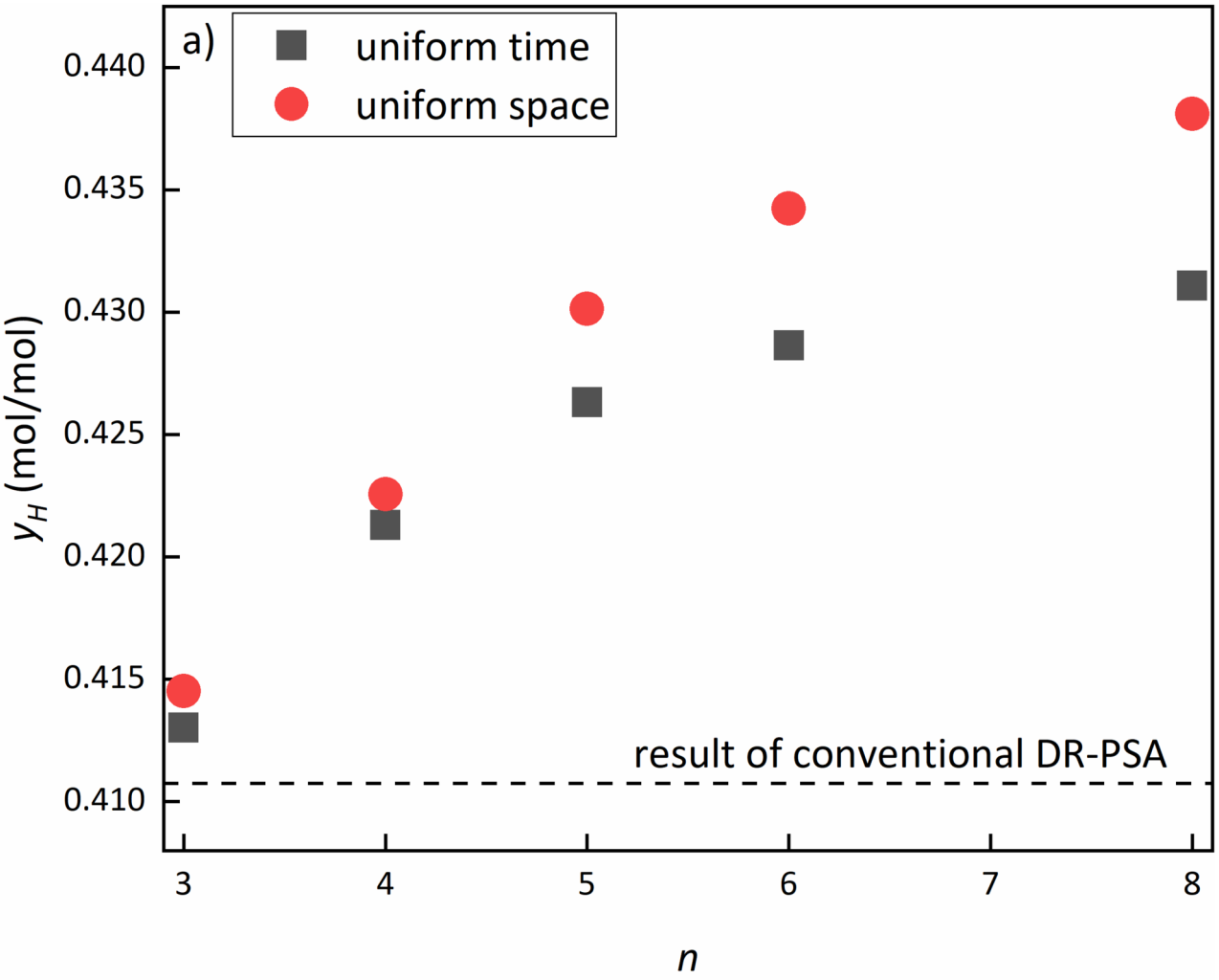

AIC_17390_Fig.6a.tif

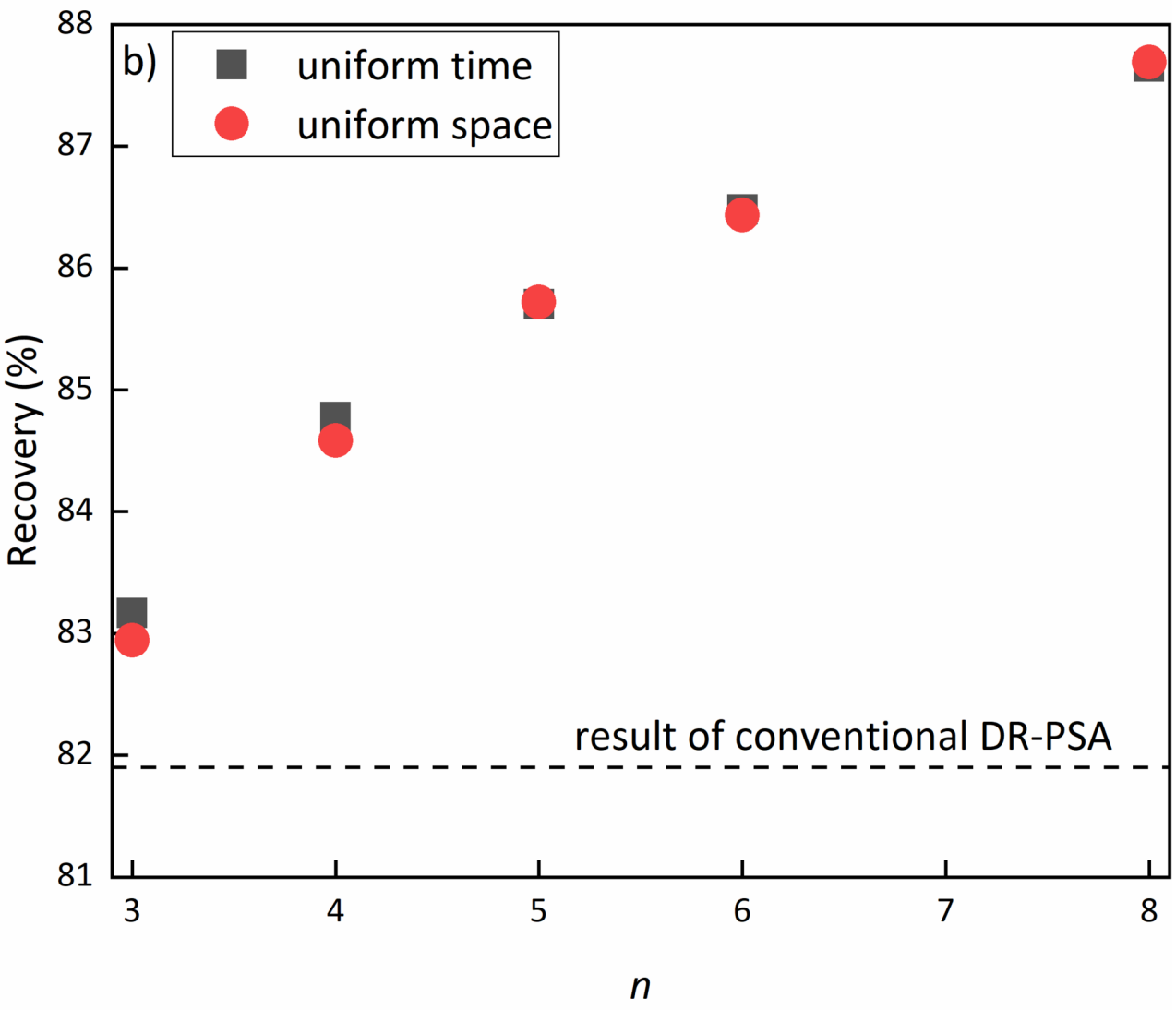

AIC_17390_Fig.6b.tif

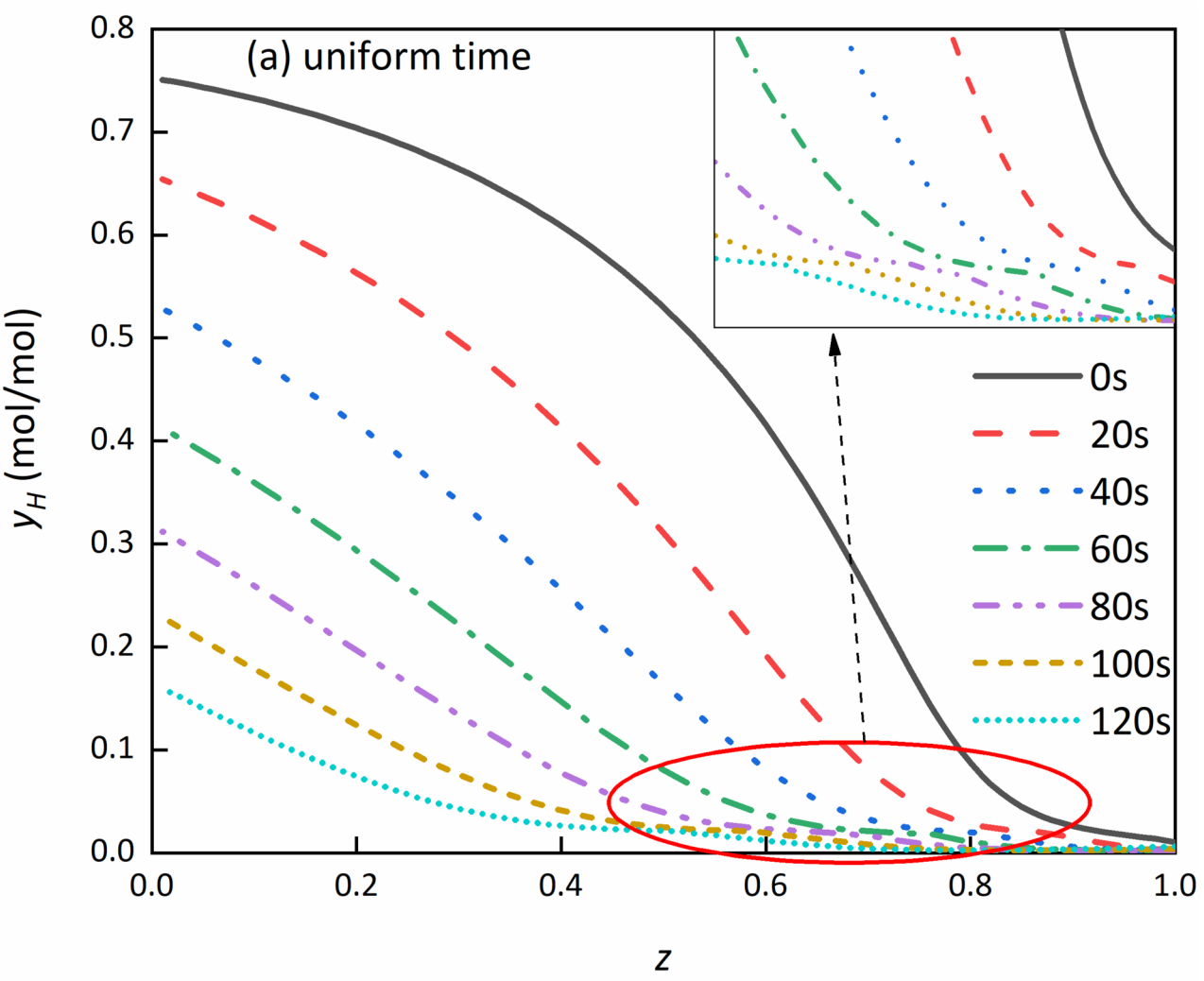

AIC_17390_Fig.7a.tif

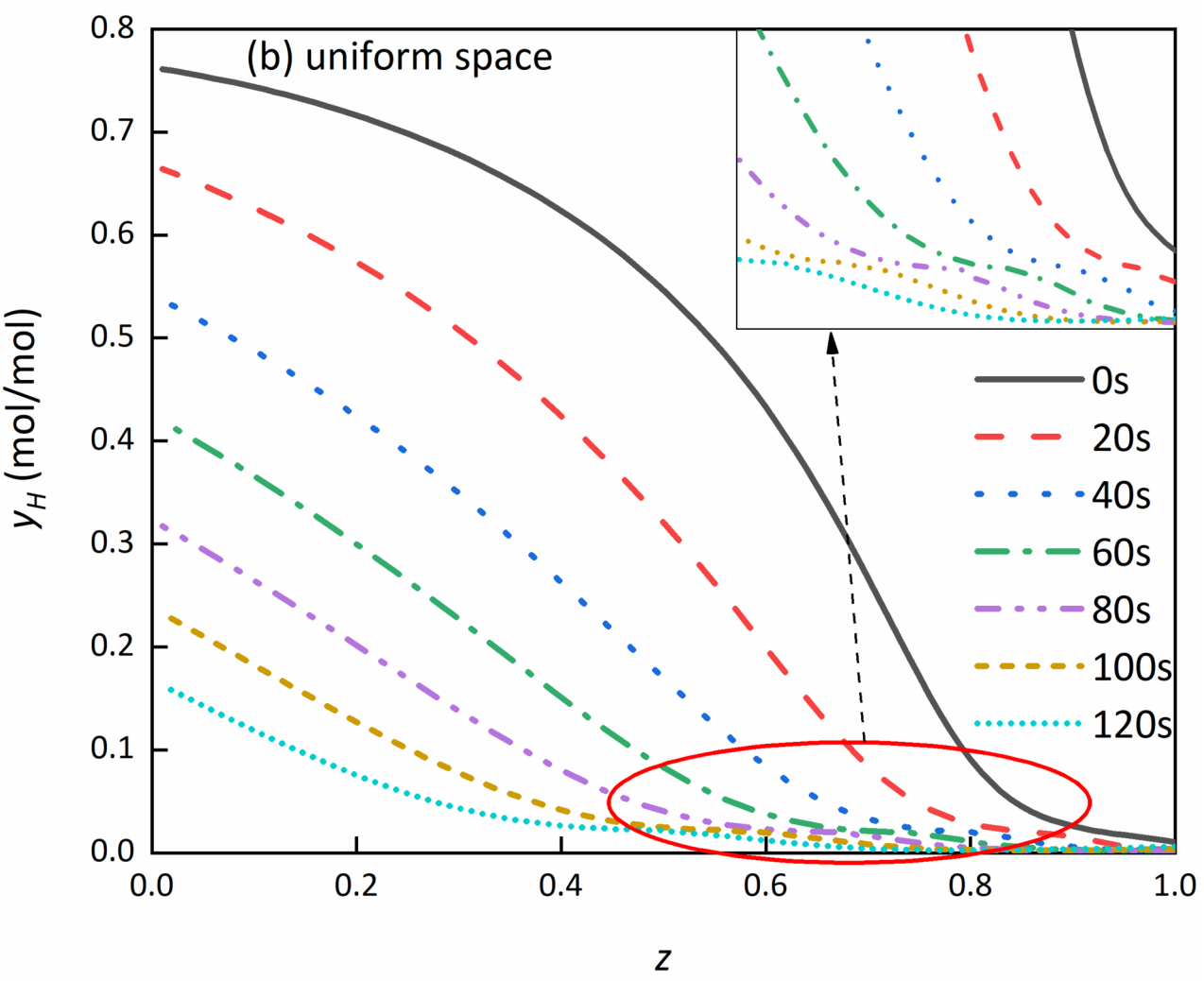

AIC_17390_Fig.7b.tif

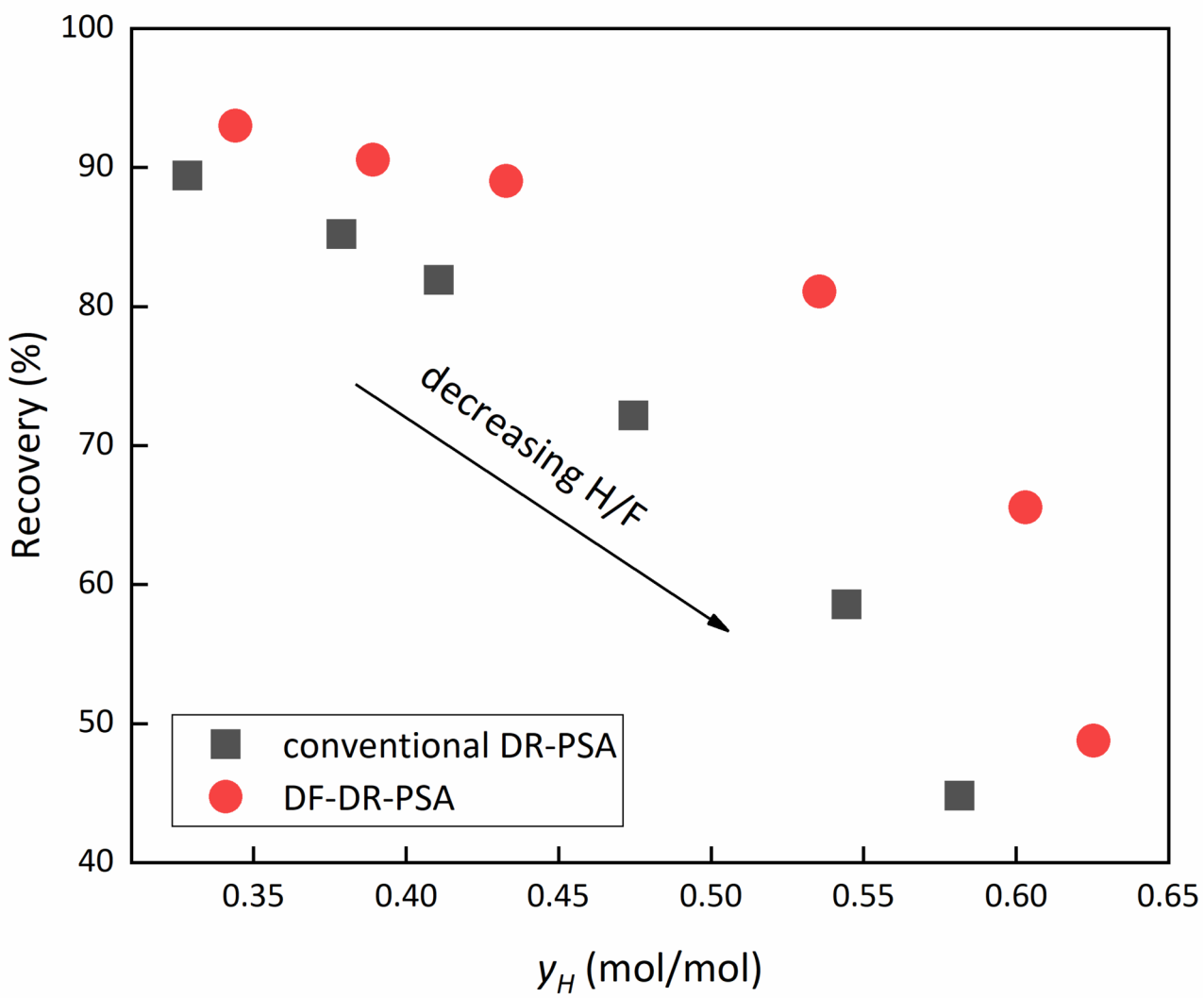

AIC_17390_Fig.9.tif

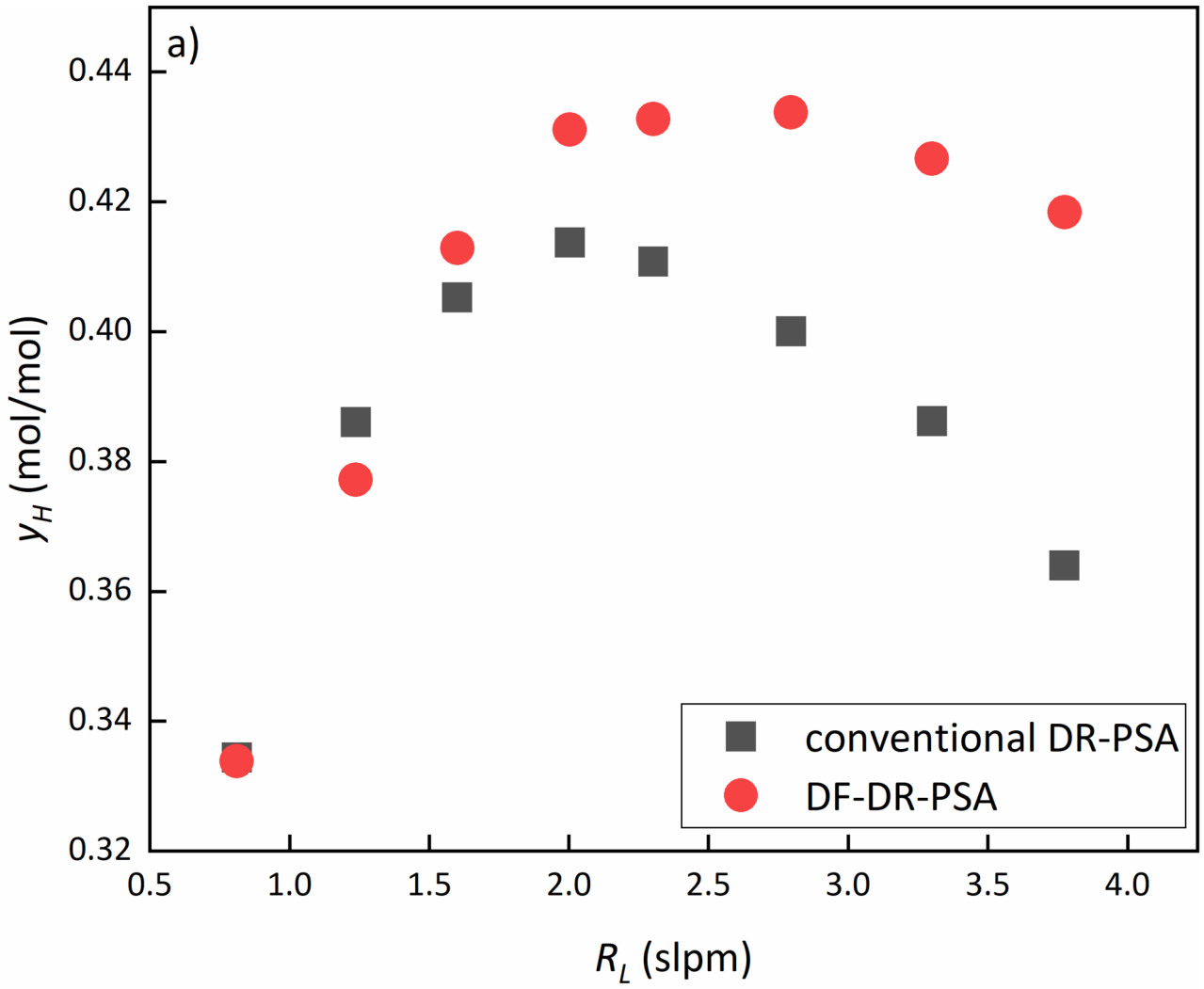

AIC_17390_Fig.10a.tif

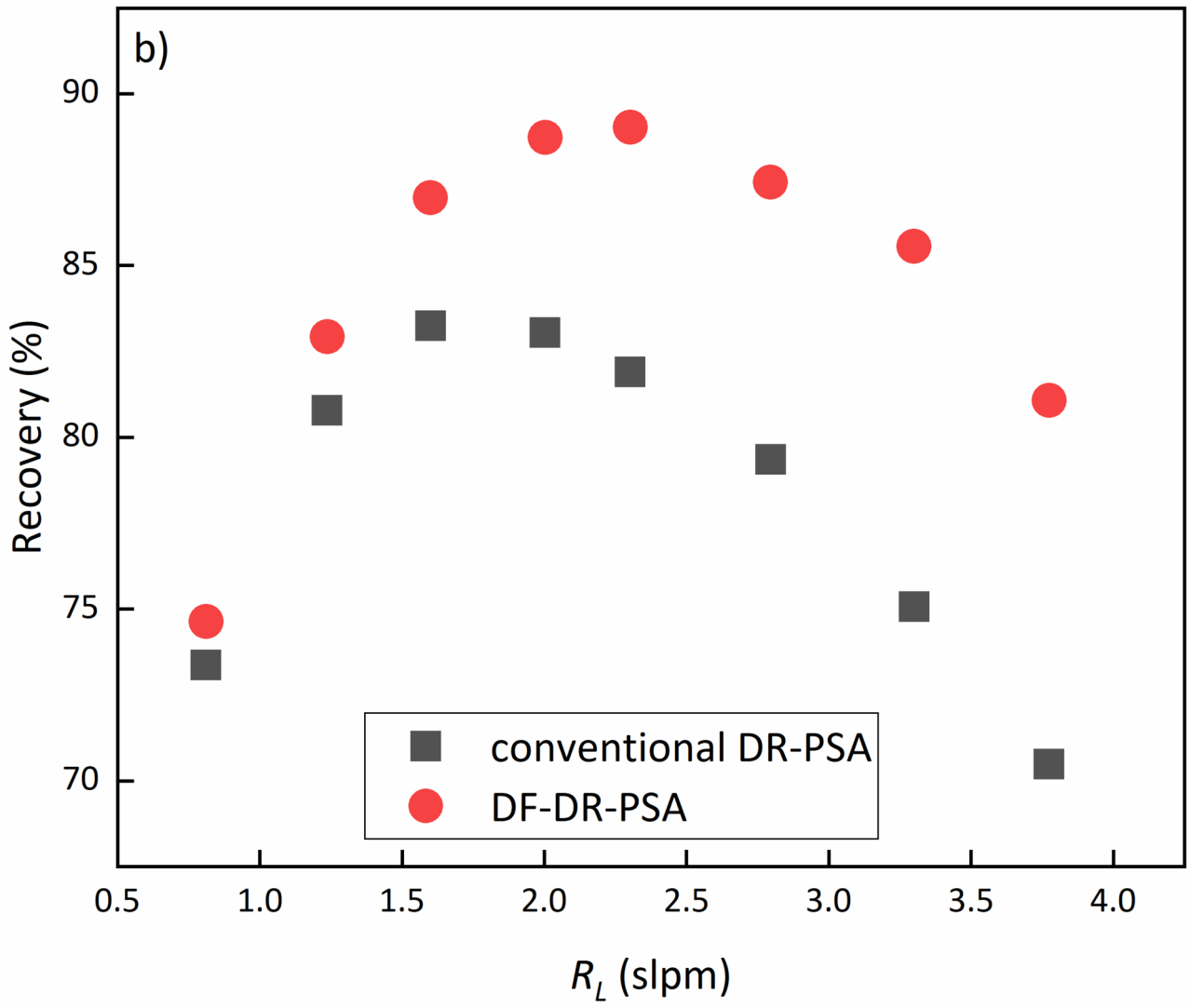

AIC_17390_Fig.10b.tif

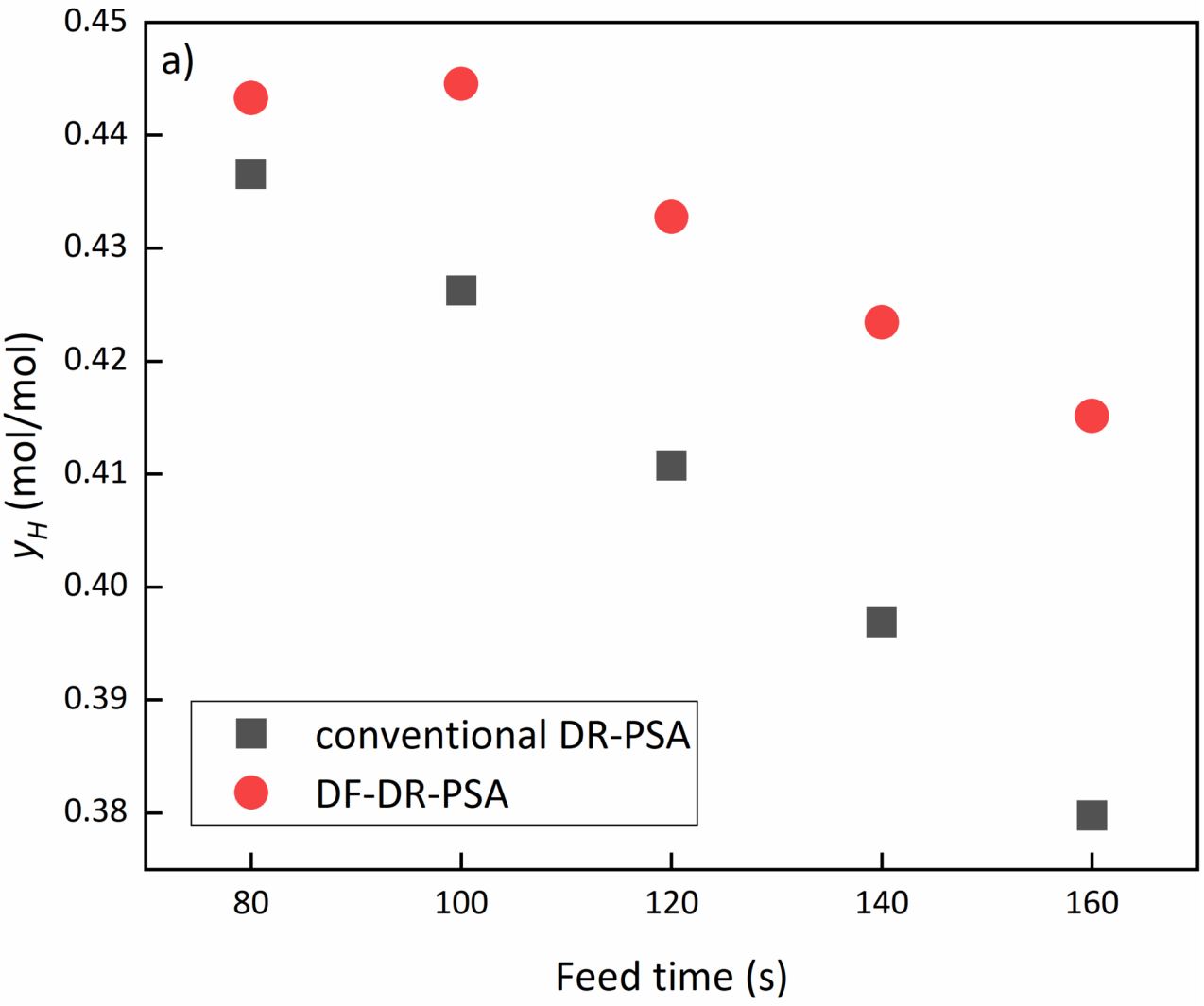

AIC_17390_Fig.11a.tif

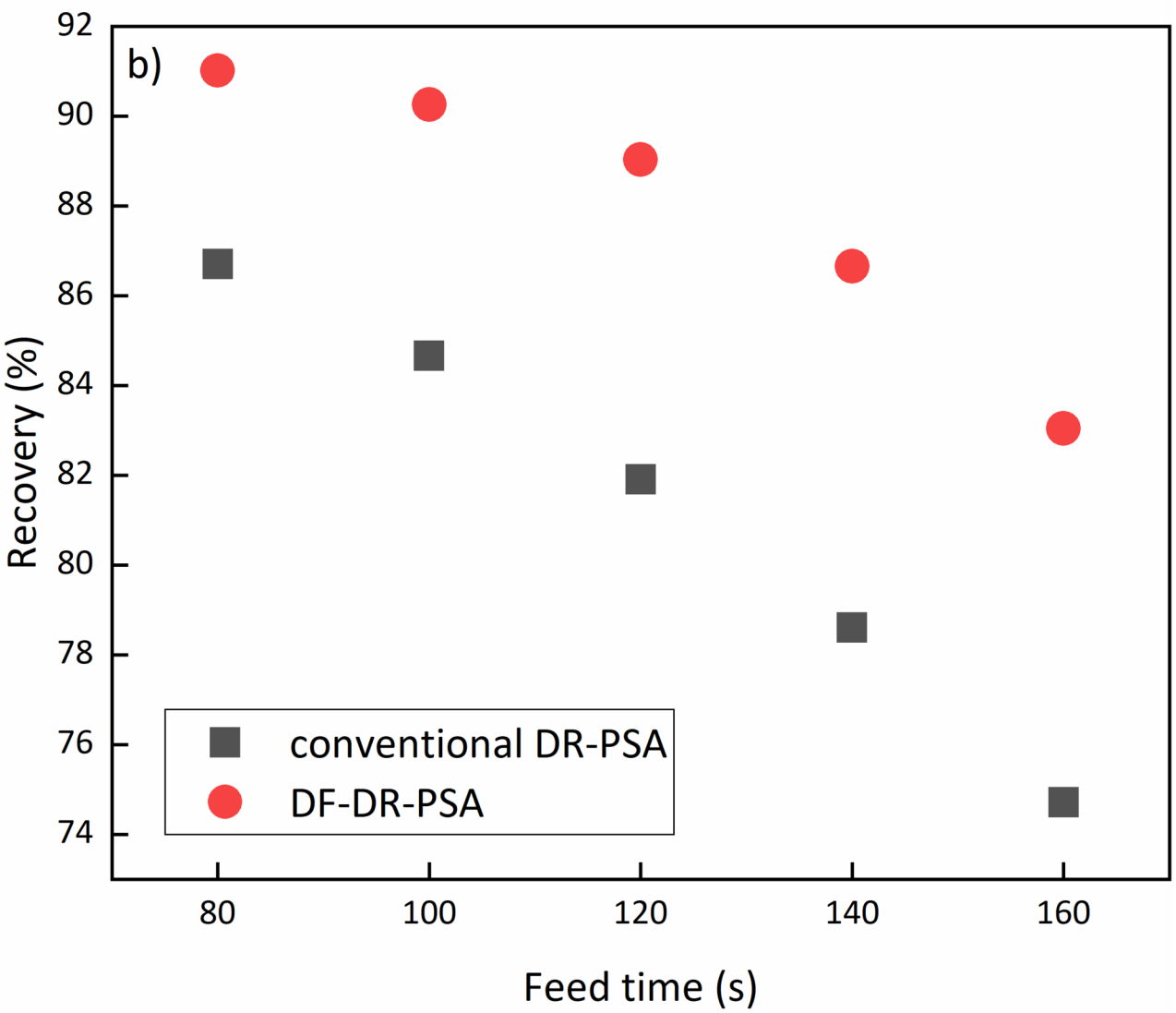

AIC_17390_Fig.11b.tif

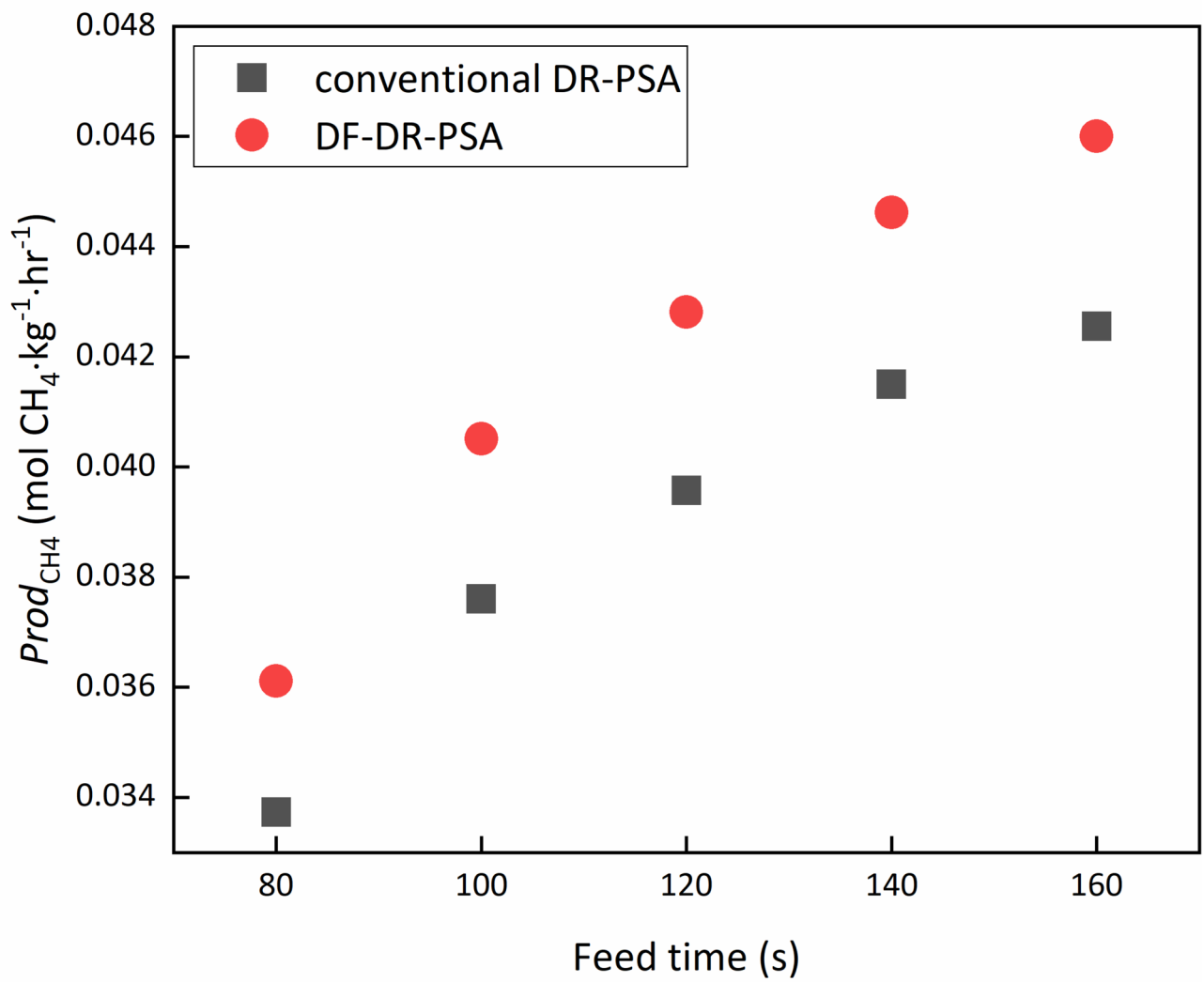

AIC_17390_Fig.12.tif

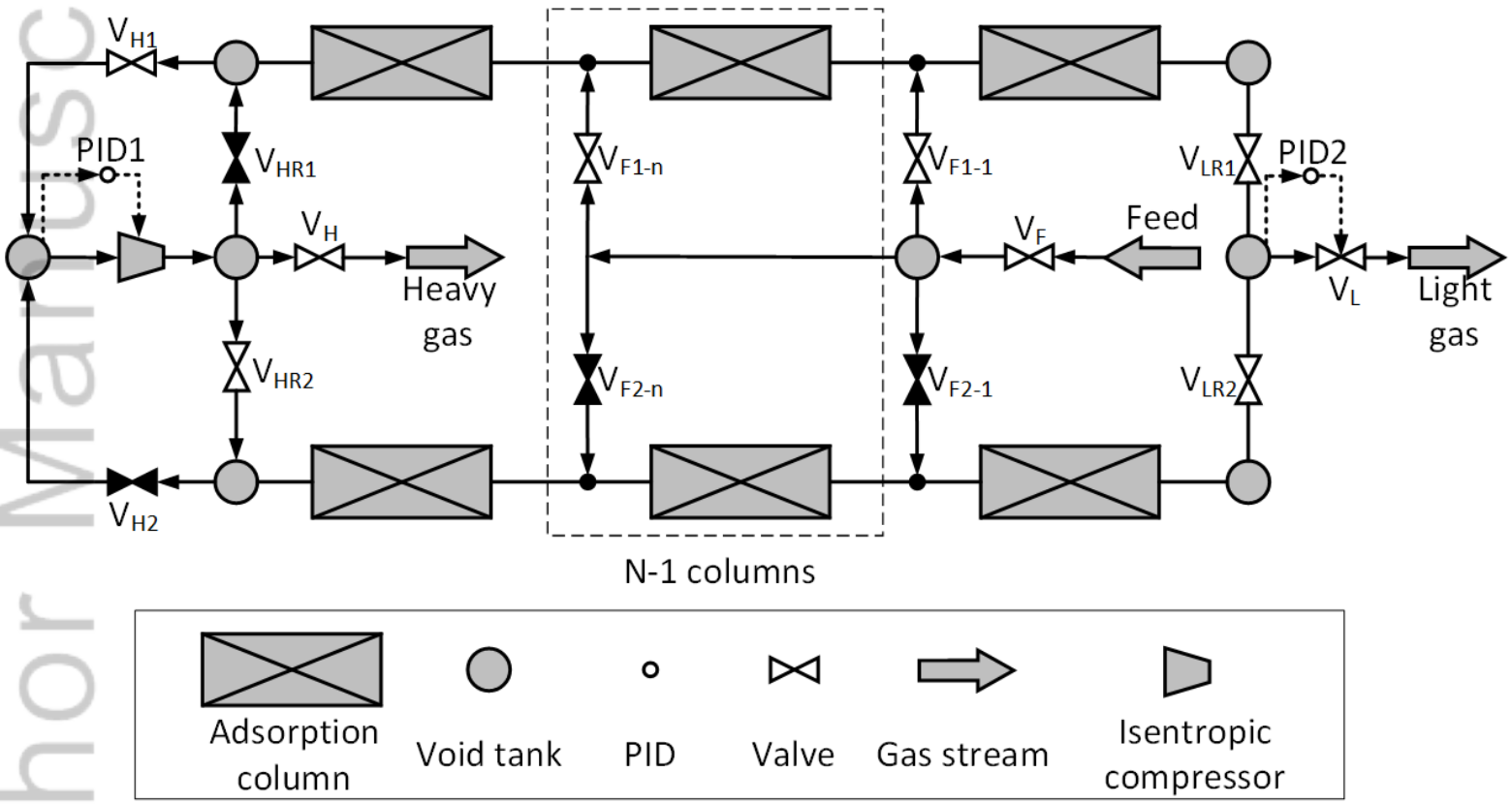

AIC_17390_FIg.3.tif

Table 1: Operational and bed model parameters used in the simulation

Parameter		Value		Unit	Source
Column parameters					
Height (H_b)		0.98		m	[29]
Column internal diameter		0.035		m	[29]
Wall thickness (W_t)		0.0016		m	[29]
Wall specific heat capacity (C_{pw})		0.5		$kJ \cdot kg^{-1} \cdot K^{-1}$	[29]
Wall-ambient heat transfer coefficient		10		$W \cdot m^{-2} \cdot K^{-1}$	[29]
Wall thermal conductivity		16		$W \cdot m^{-1} \cdot K^{-1}$	[29]
Void tank heat transfer coefficient		1000		$W \cdot m^{-2} \cdot K^{-1}$	[27]
Axial dispersion coefficient		3.5×10^{-5}		$m^2 \cdot s^{-1}$	[29]
Operational parameters					
Cycle low pressure		1.4		bar	[22]
Cycle high pressure		5		bar	[22]
Ambient temperature		293.15		K	[22]
Feed flowrate		1.25		SLPM	[22]
FE/PU step time		120		s	[22]
PR/BD step time		90		s	[22]
Adsorbent parameters					
Inter-particle voidage		0.42		m^3/m^3	[29]
Intra-particle voidage		0.65		m^3/m^3	[29]
Bulk density		435		kg/m^3	[29]
Particle radius		0.0015		m	[29]
Particle shape factor		0.752		-	[29]
Specific heat capacity		1.0		$kJ \cdot kg^{-1} \cdot K^{-1}$	[29]
Thermal conductivity		0.8		$W \cdot m^{-1} \cdot K^{-1}$	[29]
Adsorbates parameters					
		N_2	CH_4		
Mass transfer coefficient		3	1	s^{-1}	[29]
Heat capacity		29	35	$kJ \cdot kmol^{-1} \cdot K^{-1}$	[29]
Isotherm parameters	IP_1	7.30×10^{-7}	6.58×10^{-7}	$kmol \cdot kg^{-1} \cdot bar^{-1}$	[29]
	IP_2	1722	2077	K	[29]
	IP_3	1.75×10^{-4}	1.19×10^{-4}	bar^{-1}	[29]
	IP_4	1722	2077	K	[29]
Adsorption heat ($-\Delta H$)		14.322	17.27	$kJ \cdot mol^{-1}$	[22]
Gas-phase heat conductivity		0.16	0.16	$W \cdot m^{-1} \cdot K^{-1}$	[29]